National Défense
Defence nationale

MEASUREMENTS OF MULTIPATH AND ITS EFFECTS ON TERRESTRIAL VHF RADIO DIRECTION FINDING

by

William Read

DEFENCE RESEARCH ESTABLISHMENT OTTAWA
REPORT NO. 1325

Canada

December 1997
Ottawa

National Défense
Defence nationale

MEASUREMENTS OF MULTIPATH AND ITS EFFECTS ON TERRESTRIAL VHF RADIO DIRECTION FINDING

by

William Read
EW Sensors Group
Electronic Support Measures Section

DEFENCE RESEARCH ESTABLISHMENT OTTAWA
REPORT NO. 1325

PROJECT
5BD12

December 1997
Ottawa

ABSTRACT

This report details the investigation of VHF radio direction finding (DF) and the effects of multipath propagation for terrestrial paths. For this investigation, an eight-channel DF system was used to make field measurements of a transmitter as it was slowly moved along a designated route. This allowed the fine scale effects of multipath on the measured signal bearing and power to be observed – effects which had been previously observed as being noise-like in nature. Computer modelling was also used in order to develop simulations able to reproduce the effects observed in the field measurements. This has lead to the identification of the main sources of multipath, and a statistical assessment of their numbers and distribution. The computer models also allowed other factors affecting DF accuracy to be investigated which include: the transmitter-receiver path length, the size of the clearing at the DF site, the DF antenna height, and the DF algorithm. The main conclusions are that multipath is a major impediment to very high accuracy DF for terrestrial VHF DF systems, but that steps can be taken to mitigate its effects.

RÉSUMÉ

Le présent rapport expose en détails l'étude de la radiogonométrie VHF et des effets de la propagation des trajets multiples sur des voies terrestres. Au cours de cette étude, nous avons utilisé un système de radiogonométrie à huit canaux pour faire des mesures, sur le terrain, à l'aide d'un émetteur qui se déplaçait lentment le long d'une trajectoire choisie. Cela a permis d'observer la structure fine des effets causés par les trajets multiples, sur le gisements et la puissance du signal mesurée, des effets déjà identifiés comme étant semblables à un bruit. Nous avons aussi utilisé des modèles informatiques pour élaborer des simulations capables de reproduire les effets observés lors des mesures sur le terrain. Cela nous a mené à l'identification des sources principales de trajets multiples, et à une évaluation statistique de leur nombre et de leur distribution. Les modèles informatiques nous ont également permis d'étudier d'autres facteurs affectant la précision de la radiogonométrie y compris: la longeur de trajet entre l'émetteur et le récepteur, le dégagement du site de radiogonométrie, la hauteur de l'antenne radiogonométrique, et le choix de l'algorthme radiogonométrique. En conclusion, les trajets multiples sont des obstacle importants à l'atteinte d'une très grande précision des systèmes radiogonométriques VHF terrestres, mais il est possible de prendre des mesures pour atténuer ces effets.

EXECUTIVE SUMMARY

Improvement of communications radio direction finding (DF) accuracy is a high priority for the Canadian and Allied Forces. To this end, research in advanced DF techniques has been carried out worldwide over the last two decades with the view of taking advantage of advances in DF algorithms as well as the capabilities of modern processing technology.

At the Defence Research Establishment Ottawa (DREO), a series of field trials were carried out to quantify the effects of multipath propagation during the Spring of 1995. The field measurements were made using an experimental eight-channel VHF DF system (the Osprey System). These trials were a continuation of multipath research carried out at DREO and reported previously. They were carried out in support of the Canadian Forces for the improvement of land tactical VHF/UHF DF accuracy, and in support of TTCP QTP-18 (now called TTCP EWS TP-2) to investigate environmental effects on a VHF DF system.

This report discusses and analyzes the results of the field trials with the goal of developing a comprehensive understanding of the effects of multipath propagation on radio direction finding. The first step in this analysis was to examine the collected data and identify the features that could be attributed to multipath. The most notable of these features was the ripple-like perturbations in the power and bearing measurements which occurred when the transmitter was slowly moved. The cause of these perturbations was primarily due to the changing phase differences between competing signal paths as the transmitter was moved. Another important observation was that the ripple-like perturbation in the bearing measurements were range dependent which reduces the effectiveness of on-site DF antenna array calibration.

In deriving a simple model to explain the ripple effects, it was found that the spatial frequency of this ripple could be used to approximately locate sources of multipath. Conversely, spatial frequency analysis using the Fourier transform provided a means of isolating the effects of multipath sources near the transmitter from sources near the receiver or along the direct signal path, as well as from measurement errors introduced due to mutual coupling, antenna array equalization errors, instrumentation bias, etc.

Analysis of the data with or without spatial frequency analysis was not sufficiently accurate for this study, so computer models, which had been developed and reported previously, were introduced. These models were adjusted to best imitate the

field trial data (in a statistical way) in simulations of the field measurements. From these simulations, the most significant source of multipath was identified as trees surrounding the transmitter, the receiver, and along the direct signal path. The number of significant multipath sources affecting the field trial measurements was assessed to be well in excess of 100.

The computer models were also used to quantify, to some extent, factors which affect DF accuracy which include: the transmitter-receiver path length, the size of the clearing at the DF site, the DF antenna height, and the DF algorithm.

The main conclusion from this study is that multipath propagation is a serious obstacle to very high accuracy (0.1° RMS) terrestrial VHF DF, but that improvements over what is achieved with current systems ($\gg$ 1° RMS) are possible. Various well established practices for strategic DF systems, such as choosing the clearest DF site and raising the DF antenna array as high as possible above the surrounding vegetation and terrain, can greatly reduce the effects of multipath. Although difficult to implement for covert tactical systems, the consequences of ignoring these practices needs to be weighed when choosing a DF site.

Based on the findings in this study, there are several areas of research and development which could be pursued to achieve improved accuracy for tactical VHF DF systems. One area is the improvement of calibration approaches to allow rapid characterization of the multipath sources around the DF antenna. A second area is the investigation of airborne DF platforms, since the height advantage could yield accuracies approaching 0.1° RMS. And finally, the third area is the improvement of DF algorithms which includes:

1. developing terrain modelling to correct for DF errors caused by large easily identified terrain features such as forests, hills, mountains, etc.;

2. modifying the noise model used by the DF estimator to properly reflect multipath clutter generated near the DF array, transmitter, and along the direct signal path, by smaller objects such as small groves, isolated trees, bushes, etc.; and

3. incorporating modulation dependent techniques to improve co-channel performance.

TABLE OF CONTENTS

LIST OF FIGURES

LIST OF TABLES

1.0 INTRODUCTION

Improvement of communications radio direction finding (DF) accuracy is a high priority for the Canadian and Allied Forces. To this end, research in advanced DF techniques has been carried out worldwide over the last two decades with the view of taking advantage of advances in DF algorithms as well as the capabilities of modern processing technology. Central to this approach is the N-channel digital beamformer, one possible version of which is shown in block diagram form in Figure 1. The main advantage of this approach is that the phase and amplitude measurements from each antenna are available for analysis. This maximizes the information available about the incoming radio signal which allows multiple signal DF (superresolution) to be performed, or distortion of the received wavefront (compared to theoretical expectations) to be measured.

In recent years it has become evident that multipath propagation can severely degrade the accuracy of tactical VHF DF systems operated over land. To investigate the effects of multipath on DF, an eight-channel hardware realization of Figure 1, called the Osprey System, was set up at DREO. A series of field measurements were carried out with this system during the fall of 1992 and the spring of 1993, and reported in [1]. These trials confirmed that under good conditions (i.e. high signal-to-noise ratio signals, no wind, properly calibrated equipment, etc.), multipath is a dominant source of error. The trials also showed that the DF bearing errors induced by multipath were random as a function of transmitter azimuth and likely range as well. The implication of this result was that the number of sources of multipath was large and the multipath environment complex.

In the spring of 1994, a second set of measurement trials was carried out in the Ottawa area to further investigate the random nature of multipath. The measurement data was then analyzed and further insight into the multipath phenomena was gained. However many questions still remained unanswered, and since mounting a massive new measurement campaign to measure the effects of multipath under every conceivable condition and at every conceivable location was clearly impractical, other approaches were necessary to complement the measurement data.

The approach that was actually adopted was to simulate the multipath environment on a computer using theoretical models developed previously [2]. These models made it possible to simulate environments made up of large numbers of multipath sources ranging from small scattering sources to large reflecting and shadowing sources. A technique was then developed to allow the various sources to be distinguished based on N-channel

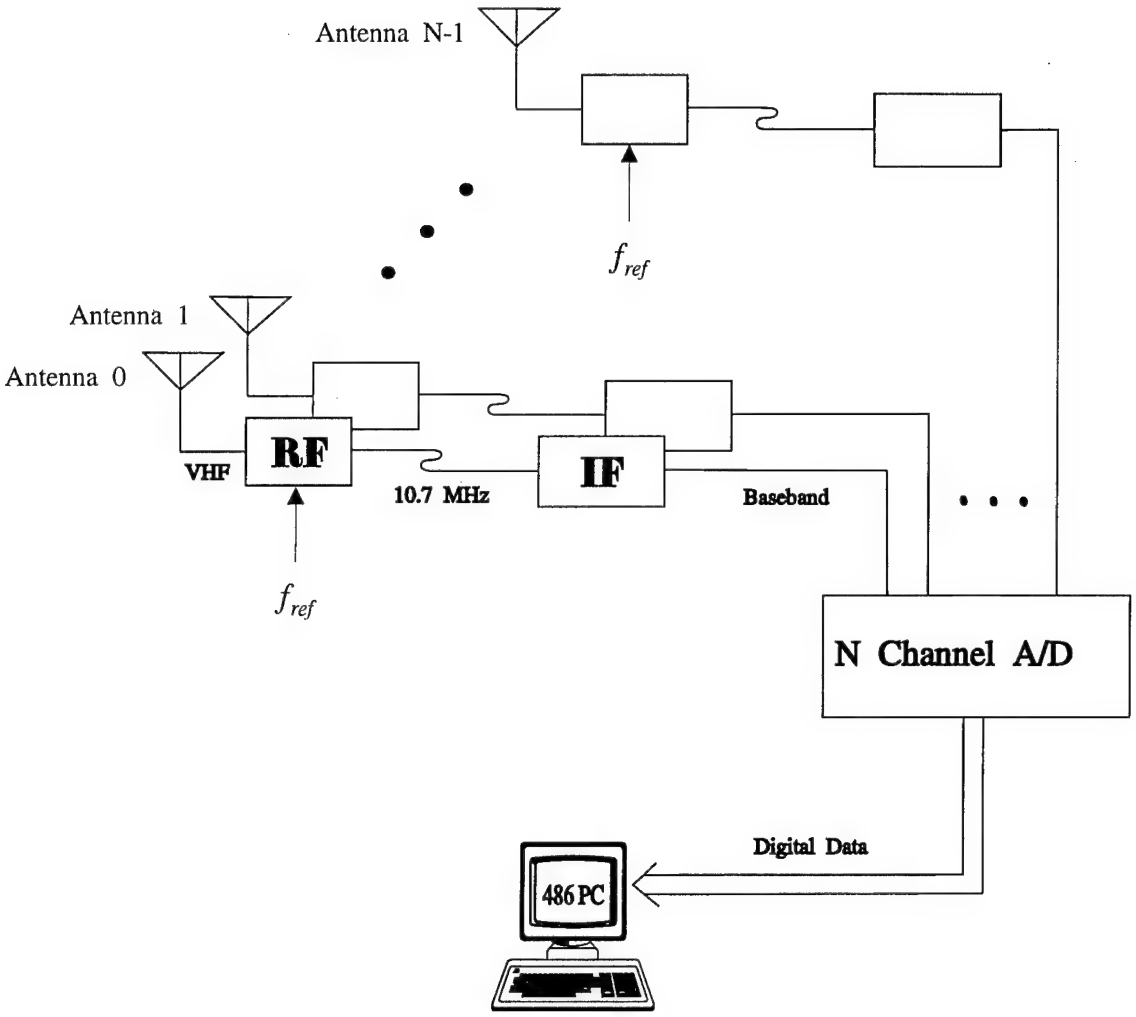

Figure 1: Experimental N channel DF system block diagram.

receiver measurements. This technique was then applied to the measured field trial data and used to determine the most appropriate size and shape of multipath source. From this, it was then possible to assess the numbers and distribution of multipath sources as well as examine various factors which affect DF accuracy, such as the transmitter-receiver path length, the size of the clearing at the DF site, the height of the DF antenna array, and the DF algorithm.

This report is arranged in seven main sections including this first section. Section 2 describes the experimental setup including a brief description of the Osprey hardware, some processing considerations, the site surrounding the Osprey system, the transmitter hardware, the transmitter sites, and the measurement test plan. Section 3 describes the results of the field measurements with some preliminary analysis. Section 4 discusses the spatial frequency content of the measurement data and how it was generated. This section also describes how spatial frequency can be used to localize sources of multipath and remove the effects of various sources of error from the data. Section 5 introduces the multipath simulation models and then refines these models to match the results from the field measurements. Based on simulation results from the refined models, the size, numbers, and distribution of multipath sources is estimated. Section 6 uses simulations to examine the effect of changing the transmitter-receiver path length, clearing the DF site of sources of multipath, raising the DF antenna array, and selection/modification of the DF algorithm. Finally, Section 7 provides the conclusions and recommendations.

2.0 EXPERIMENTAL SETUP

2.1 DF System

The Osprey antenna system consists of a linear array of 2.9 meter dipole whip antennas spaced at intervals of 2 meters. The antennas are mounted on a 15 meter long fiberglass truss. The truss is in turn supported 2 meters off the ground by a large pivot at the center, enabling the truss to be rotated manually through 360°. Adjustable supports at either end of the truss are used to prevent sagging over the length of the truss. For the experiments discussed in this report, the truss was left in the position shown in Figure 2 and the 0° azimuth bearing reference was also as shown.

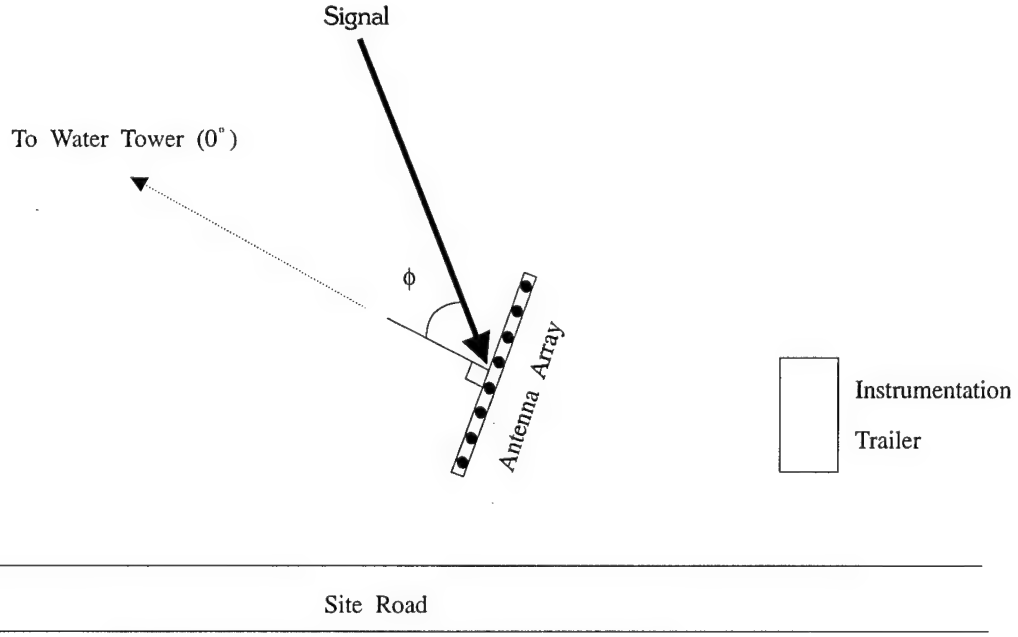

Figure 2: Physical layout of field trial DF site.

For alignment purposes, the 0° bearing reference was chosen to correspond to the bearing of a water tower (not shown in Figure 2) located at a range of 990 meters from the antenna system which provided a useful map and visual marker. The alignment accuracy was assessed to be ±1°.

2.2 Processing Considerations

The conversion of the radio frequency (RF) antenna voltages to baseband digital in-phase and quadrature (IQ) formatted data, and then to direction estimates followed the same approach outlined in [1]. The one exception was the manner by which the unknown channel gain and phase offsets were estimated.

To determine these unknown offsets, a CW reference transmitter was positioned at 61 meters from the center of the antenna array and at a bearing of 0° in azimuth. Measurements of this signal taken using the Osprey system were then corrected so that the measured signal phase and amplitudes were the same on each channel. The same amplitude and phase corrections were then applied to subsequent measurements of transmitters at other bearings. This process is herein referred to as channel equalization – not to be confused with passband frequency equalization which was unnecessary for the Osprey receivers.

For the field measurements, the reference transmitter was operated at 62.5 MHz, but offset by 40 Hz from the frequency of the mobile CW transmitter. This was close enough in the receiver passband that the equalization for both frequencies was the same, but far enough apart that the two signals could be easily separated using the IQ frequency domain processing technique described in [1].

A problem with the equalization approach described here is that it assumes the propagated reference signal can be represented by a plane wave when it is intercepted by the DF antenna array. In reality, this assumption is not true for three reasons. First, the close proximity of the transmitter causes the received radio wave to be slightly spherical in shape. This curvature introduces constant phase and amplitude errors which are symmetrical with respect to the center of the array, i.e. the first and last antennas will have identical phase and amplitude errors. A consequence of this symmetry is that for a *single* transmitter, no DF errors occur.

The second reason is that reflections from the ground and the surrounding environment produce unknown distortions in the shape of the received radio wave. These distortions cause asymmetric phase and amplitude errors that can be minimized by ensuring the region in and around the direct signal path is relatively flat and clear (i.e. free of multipath sources).

The third reason is mutual coupling between the antennas of the DF array which also

causes distortions to the shape of the received radio wave. For the Osprey antenna array, the bearing errors introduced by mutual coupling are acceptably small for transmitter bearings between $-60°$ and $+60°$ [1].

Despite these problems, the DF errors introduced using this channel equalization method are not serious when measurements against a single transmitter are considered, nor do they provide an impediment to the multipath analysis carried out in this report. Additionally, a big advantage of this method is that it is very simple and it allows the reference transmitter to be left on during field measurements so that receiver problems can be identified

2.3 DF Site Layout

The layout of the DF site was as shown in Figure 2. This site was far from an ideal site due to the proximity of the surrounding trees (e.g. Figure 34 shows the approximate location of many of the larger trees), bushes, wire fences, ditches, etc., which are all obstacles that according to [3] can cause errors in bearing measurements. This site was chosen, however, because it was easily accessible and reasonably secure.

2.4 Transmitter Sites

The reference transmitter was located 61 meters from the array at a bearing of $0°$. The transmitting antenna used was a 2.9 meter whip dipole (identical to the type used in the Osprey DF array) mounted 1.2 meters above the ground. The antenna was fed directly by a frequency synthesizer located in the instrumentation trailer. Double shielded cables were used to feed the synthesizer signal to the antenna to minimize RF leakage.

A mobile transmitter was also used and it was operated on the roads in and around the DREO site (e.g. Figure 4a), and on Riddell Road which was 5-6 kilometers from DREO (e.g. Figure 12a). The transmitter equipment was placed in either a minivan or station wagon for the trials and consisted of a 12 VDC to 120 VAC invertor, a frequency synthesizer, and a power amplifier capable of generating a CW signal of up to 3 watts. The antenna was a 2 meter whip monopole antenna which was mounted on a sled. The sled was either attached to the roof of the transmitter vehicle, or pulled along the ground. When pulled along the ground, the antenna was fed from the power amplifier by a single shielded cable 85 meters in length. For the roof mount configuration, a short single

shielded cable was used.

2.5 The Test Plan

The field trials consisted of 8 days of data collection, beginning in April and ending in May 1994, as summarized in Table 1. The term "measurement set" used in the table and the rest of this report is defined as a recorded set of digital data covering a single continuous period of time. The routes followed by the mobile transmitter for each measurement set are shown in Figures 4a-7a, 9a, 11a, 12a, 14a and 16a. For logistical reasons the chosen routes followed local roads.

Table 1: Field Trial Measurement Set Summary

Measurement Set	Date	Transmitter Antenna	Time Duration
1	April 8	Ground (f)	16:23
2	April 8	Ground (r)	16:23
3	April 12	Ground (f)	16:23
4	April 12	Ground (r)	16:23
5	April 19	Ground (stationary)	14:20
6	April 19	Vehicle	14:20
7	May 5	Ground (f)	14:20
8	May 5	Ground (r)	14:20
9	May 5	Ground (f)	14:20
10	May 5	Ground (r)	14:20
11	May 16	Ground (f)	14:20
12	May 16	Ground (f)	14:20
13	May 16	Ground (f)	14:20
14	May 16	Ground (f)	14:20
15	May 18	Vehicle	17:04
16	May 27	Ground (r)	14:20
17	May 30	Vehicle	14:20
18	May 30	Vehicle	14:20

For each trial, the Osprey system was setup to automatically and continuously measure RF signals at 62.5 MHz for specific periods of time ranging from 14 minutes 20 seconds to 17 minutes 4 seconds. Signal power levels were set so that the signal-to-noise ratio for the I and Q processed data was more than 40 dB. The sampling rate used for digitizing the baseband analog data was 1000 Hz for each channel.

For processing purposes, the data in each measurement set was divided into blocks of

256 points per channel representing 0.256 seconds of collection. From each channel block, a single amplitude, phase, and DF measurement was then computed.

The starting position for each route was chosen to be easy to locate on either a 1:25000 topographical map of the Ottawa area or a 1:5000 overhead photograph of the DREO site.

For measurement sets 1-4, 7-14, and 16, the mobile transmitter antenna was moved by pulling it along the ground at a rate of 0.30 meters/second. The total distance covered was typically 175-180 meters. The transmitter vehicle was located at the midpoint of the route over which the antenna was pulled and was not moved during transmissions. When the transmitter antenna was moved this way, it always passed the vehicle on the side closest to the receiver, with the minimum distance between the vehicle and antenna being 1-2 meters. Using the known transmitter velocity, the position of the transmitter could be determined to within ± 1 meter (which includes cumulative measurement errors) relative to the starting position for any time during the measurement set. The fine spacing between successive antenna positions ($0.256 \times 0.30 = 0.077$ m) was to ensure that the fine scale effects due to multipath would be observed.

Measurement set pairs (1,2), (3,4), (7,8), and (9,10), represent repeated measurements with the first number in a pair representing measurements made with the transmitter moving in one direction and the second number representing measurements made over the same route but in the reverse direction (denoted by the (f) or (r) in the third column of Table 1). The purpose of the forward-reverse pairs was to check the repeatability of the measurements, i.e. to ensure that the effects observed were spatial and not temporal in nature.

For measurement sets 6, 15, 17, and 18, the transmitter antenna was mounted on the transmitter vehicle, and driven at approximately 7 kph. Positions were determined approximately using the vehicle odometer and the known starting position, or by recording the time that landmarks visible on the map were passed. Position accuracy for these sets was considerably poorer than the other sets. This is discussed in more detail in the appropriate subsections of Section 3. The main purpose was to collect data for longer transmitter routes and ensure that the effects of multipath observed in the other data sets were not restricted to localized areas.

In measurement set 5, the vehicle was slowly driven past the transmitter antenna (which was left in a stationary position on the roadside) at an average speed of 0.3-0.4 kph. The purpose of this test was to investigate the effect of the transmitter vehicle on

the measured results.

Measurement set 12 was a continuation of measurement set 11 (in terms of transmitter position). The same comment is true for measurement sets 13-14, and measurement sets 17-18. Additionally, sets 11-12 and 13-14 represent measurements made for the same azimuth angles, but at two different ranges.

The transmitter frequencies were 62.5 MHz for the mobile transmitter and 62.5 MHz - 40 Hz for the reference transmitter. Measurements were made when the weather conditions were reasonable, i.e. no rain and low winds. Temperatures during the measurements ranged from $4 - 10°C$ in April to $12 - 20°C$ in May. Ground conditions were wet in April due to the spring runoff, becoming drier throughout May.

3.0 MEASUREMENT OBSERVATIONS

The field trial measurements are discussed according to date in the following sections. The discussion does not include the measurements for the reference transmitter since the receivers operated without any malfunctions and receiver drift was negligible. For example, Figure 3 shows the drift in the reference transmitter measurements that occurred during measurement set 1 (April 8). Figures 3a and b show phase and power drifts respectively, while Figure 3c shows the bearing drift. The power levels shown in this and any following figures is displayed in dB relative to the average signal power. Most of the observed variations are due to co-channel interference between the reference transmitter and the mobile transmitter (e.g. compare Figure 3b to Figure 4b). Even so, the corresponding RMS bearing error was only 0.03°. Since multipath causes errors on the order of one degree or more, drift effects could be ignored.

3.1 April 8

In [1], multipath was found to produce random errors in the DF error measurements as the transmitter was moved to successive positions spaced 50 meters apart. Measurements in March 1994 (not reported) indicated that the DF error was random for 10 meter spacings, but beginning to show some predictability for 1 meter spacings. Given this, measurements were taken continuously as the transmitter was moved at a slow rate 0.30 m/s in order to properly observe the fine structure of the error variations. Figure 4 shows the results.

In the map shown in Figure 4a, the numbers beside the arrows indicate the corresponding measurement set. As indicated on the map, both measurement sets represent the same transmitter route except the directions were opposite. To facilitate easier correlation between the results for the two data sets shown in Figures 4b and c, the distance shown is the distance travelled by the transmitter measured with respect to the starting position for measurement set 1. In addition, the results for measurement set 2 have been offset downwards (2° and 10 dB respectively) in Figures 4b and c.

Several conclusions can be drawn from the results. First, given the good agreement between the two data sets, the dominant source of error was spatial in nature. Temporal error sources (noise, wind shaking the DF antennas, receiver drift, etc.) would cause random errors over time and which would not correlate with transmitter position. Spatial

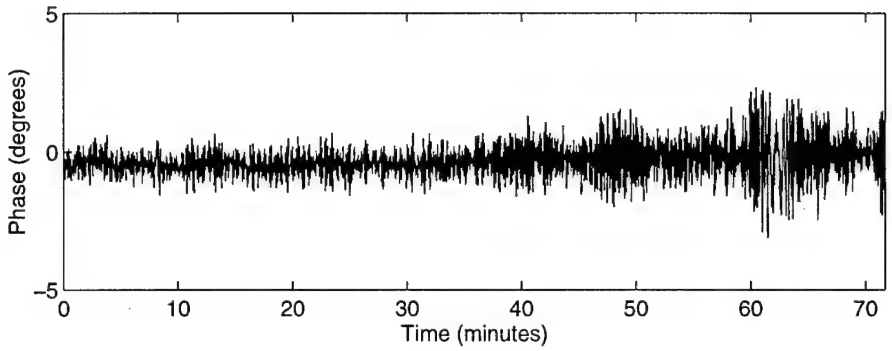

(a)

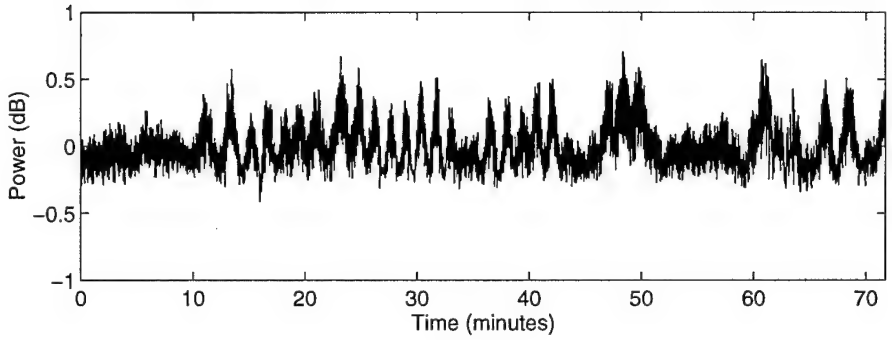

(b)

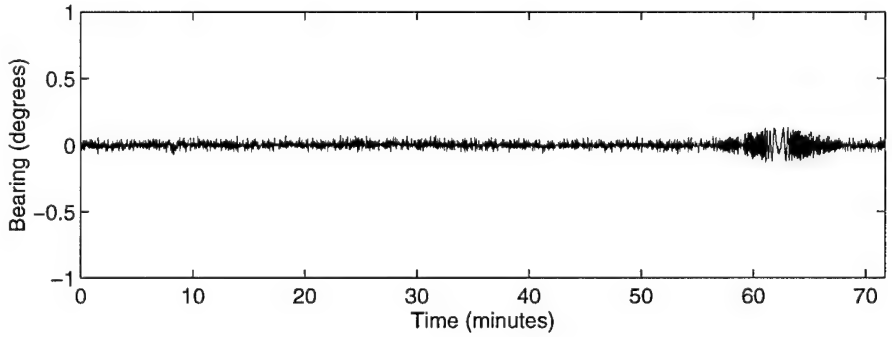

(c)

Figure 3: Drift effects measured using the reference transmitter during measurement set 1 showing (a) the phase difference between channels 1 and 2, (b) the signal power measured in channel 1, and (c) the measured bearing.

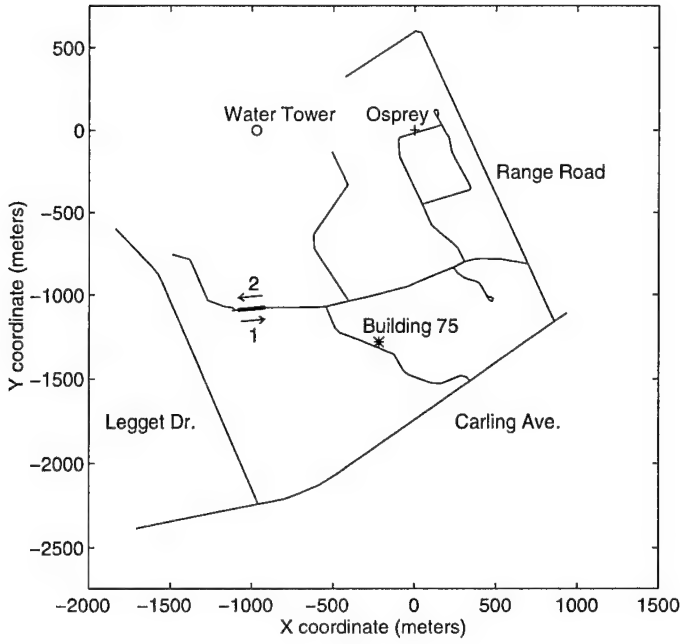

(a)

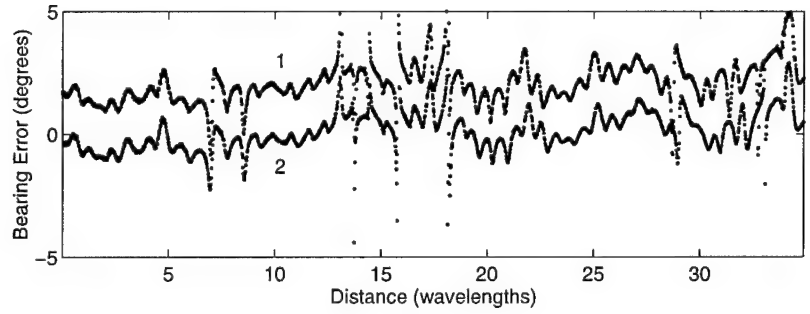

(b)

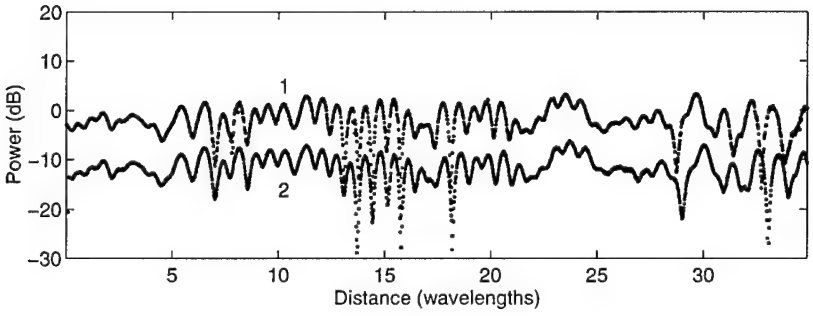

(c)

Figure 4: Measurements taken on April 8 showing (a) a map of the transmitter route, (b) the bearing errors, and (c) the received signal power (averaged for all channels).

errors (due to multipath, mutual coupling, poor antenna array equalization, etc.), on the other hand, can be repeated simply by repeating the same transmitter-receiver geometry.

The second conclusion is that the main source of error was multipath. Other than multipath and transmitter position errors, all other known error sources cause slow variations in the bearing error as a function of transmitter position. Position errors arising from estimating the true transmitter starting position on a map lead to constant bearing errors which can be ignored. Random position errors of 1 meter or less relative to the starting position, and at a transmitter-receiver ranges of 1 km or more, produce errors of less than 0.1° – too small to be significant. Position errors in conjunction with multipath effects may, however, explain the differences that do exist between the forward and reverse paths.

The third conclusion is that a noticeable portion of the multipath originates near the transmitter. This conclusion is based on two observations. First, from path loss considerations, the most significant multipath will be generated near either the transmitter and receiver. Second, the very rapid periodic fluctuations observed in Figure 4b and c imply that the multipath sources are some distance from the receiver, i.e. near the transmitter [1] (see also Section 4.0).

Possible (and easily identifiable) sources of multipath along the transmitter route include a metal gate near the start of the transmitter route, a bank of large trees along the side of the road (on the side opposite the receiver) for the middle portion of the transmitter route, the transmitter vehicle at the midpoint of the route, and the ground. Based on sheer size, the trees probably accounted for the large fluctuations in signal power and bearing which occurred at distances of $12 - 18\lambda$ along the transmitter route (where the wavelength $\lambda = 4.8$ meters).

3.2 April 12

Following an identical procedure to the measurements taken on April 8, a set of measurements was taken at a new location as shown in Figure 5a. The results from these measurements are plotted in Figure 5b and c using the same convention as in Figure 4. Although a different transmitter route was used, the characteristics of the bearing error and signal power are similar to those of April 8 (although not quite as strong), implying that either the sources of multipath are prevalent everywhere, or the apparent source of multipath was the measurement system itself (i.e. the transmitter vehicle).

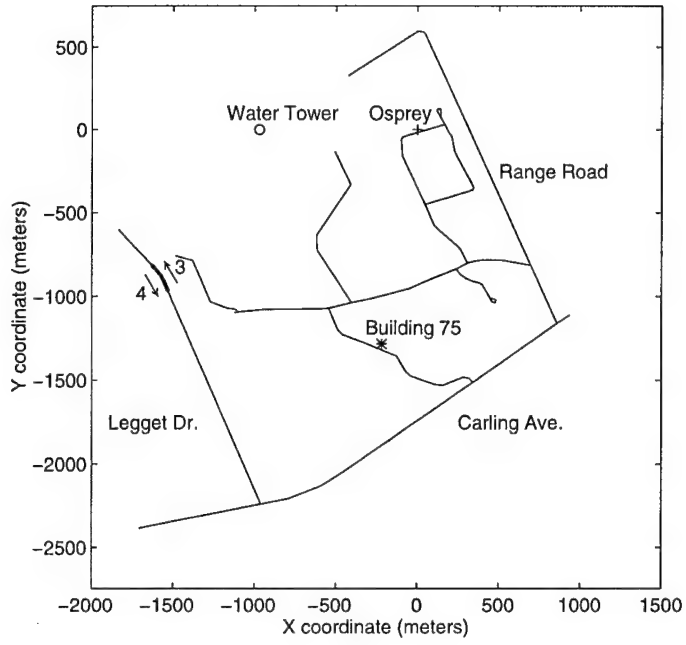

(a)

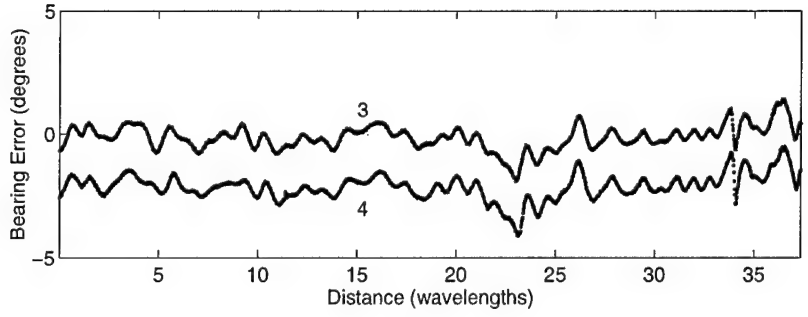

(b)

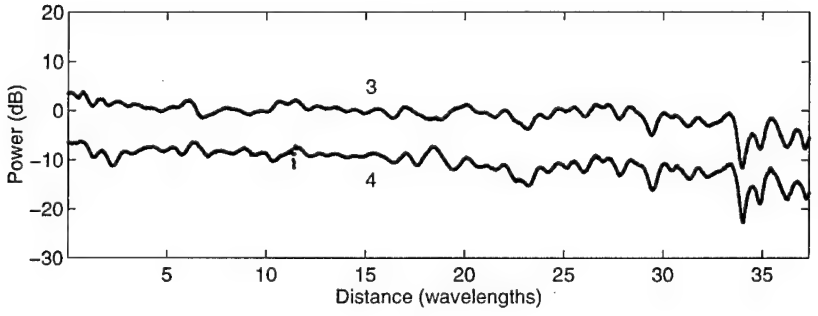

(c)

Figure 5: Measurements taken on April 12 showing (a) a map of the transmitter route, (b) the bearing errors, and (c) the received signal power (averaged for all channels).

3.3 April 19

To investigate whether the measurement system itself was a source of the observed multipath, two experiments were performed on April 19. In the first experiment, the transmitter antenna was left stationary on the ground while the transmitter vehicle was slowly driven past it at an average speed of 0.3-0.4 kph. The hollow box in Figure 6a shows the route of the vehicle. The transmitter antenna was located at the middle of the box. The results are shown in Figure 6b and c.

The dotted line indicates the point in time when the vehicle was directly beside the antenna. For logistical reasons, the vehicle was driven past the antenna on the receiver side (i.e. although relatively quiet, the road was used by other vehicles so that leaving the transmitter antenna in the middle of the road, or alternatively driving on the wrong side of the road, posed a safety hazard). This is evident in the plot of power where the power drops by 3 dB as the signal path is obstructed by the vehicle. Except while the vehicle was directly beside the transmitter antenna (within 1 m), the effects of the vehicle on bearing and signal power were too small to have caused the effects observed in the data collected on the April 8 and 12. In fact, by comparison, these results strongly suggest that the source of multipath causing the large and rapid bearing fluctuations on April 8 (particularly at distances of $12 - 18\lambda$) was significantly larger than the vehicle and at least $6\lambda = 29$ meters long, i.e. the bank of trees along the side of the road.

Given that the measurement system was not generating the observed multipath effects, a second experiment was performed to determine whether multipath was prevalent everywhere or whether it was localized to various sites. In this experiment, the transmitter antenna was mounted on top of the transmitter vehicle and the vehicle driven slowly at an average speed of 7-8 kph along the route shown in Figure 7a. Position accuracy was not a major concern since the idea was to determine whether the bearing fluctuations due to multipath occurred continuously or sporadically. Certain landmarks and the time they were passed were noted to provide a rough indication of transmitter position. The results are shown in Figure 7b and c. Note that since the transmitter positions were not known precisely during the measurements, the estimated bearing is shown in Figure 7b rather than the bearing error.

The uncertainty in transmitter position introduces a slow variation in the bearing error versus transmitter position results. To remove these slow variations, the coefficients of a 9th order polynomial were computed for the best least squares fit to the measured

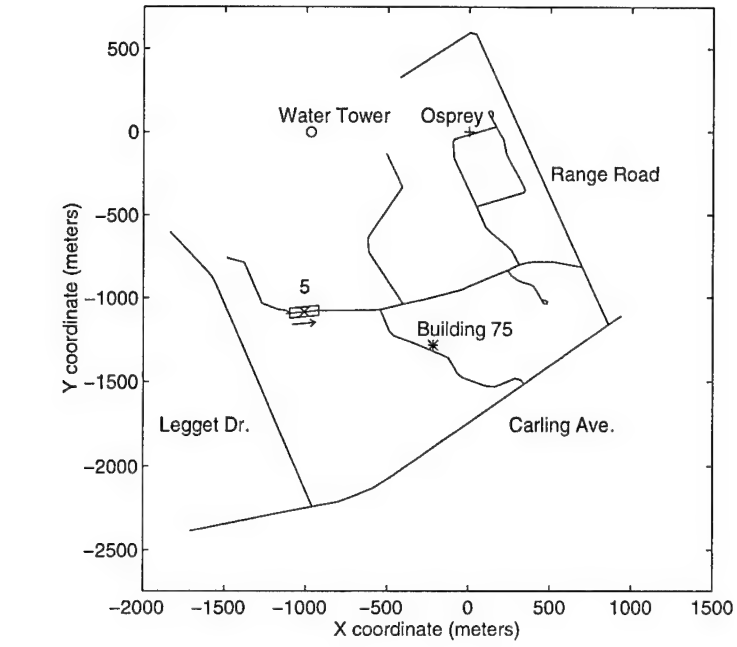

(a)

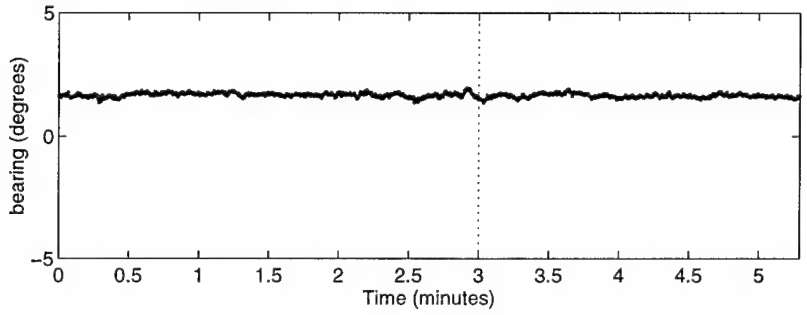

(b)

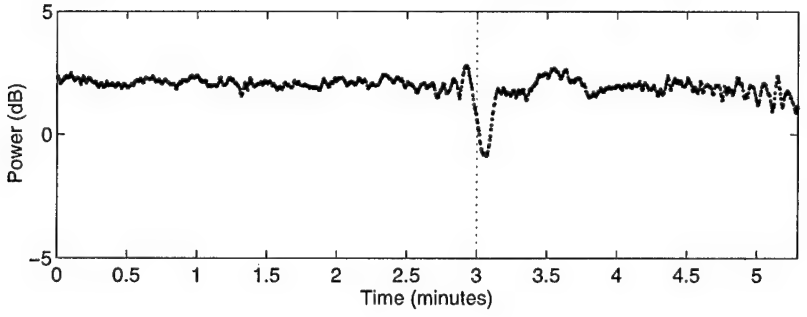

(c)

Figure 6: Measurements taken on April 19 to test for interference of vehicle showing (a) a map of the vehicle route (arrow) and the transmitter position ("x" inside box), (b) the bearing errors, and (c) the received signal power (averaged for all channels).

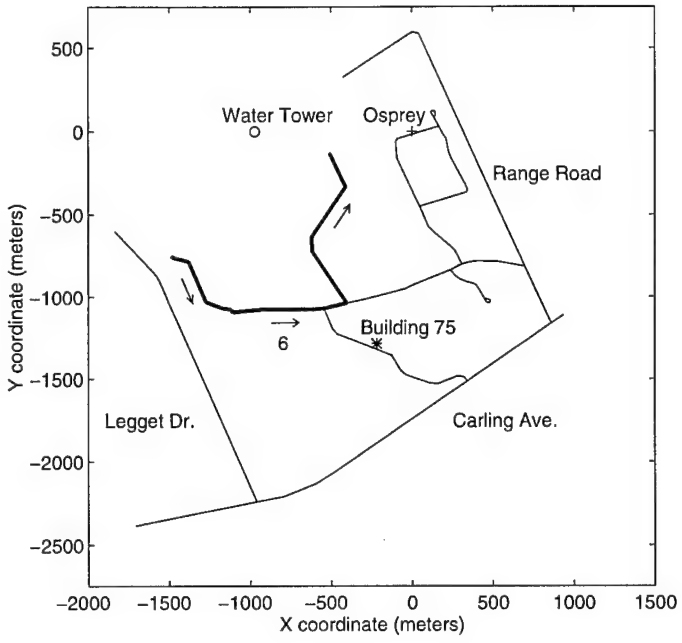

(a)

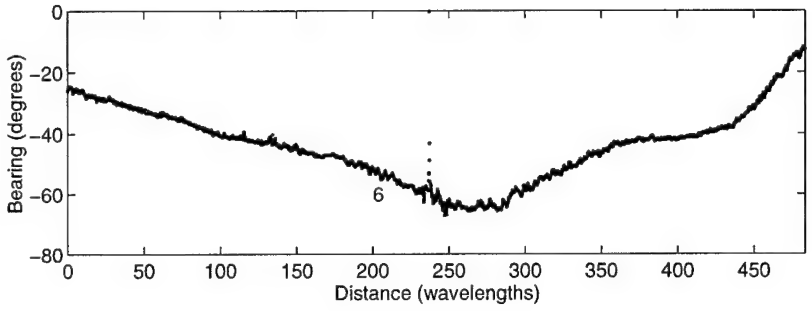

(b)

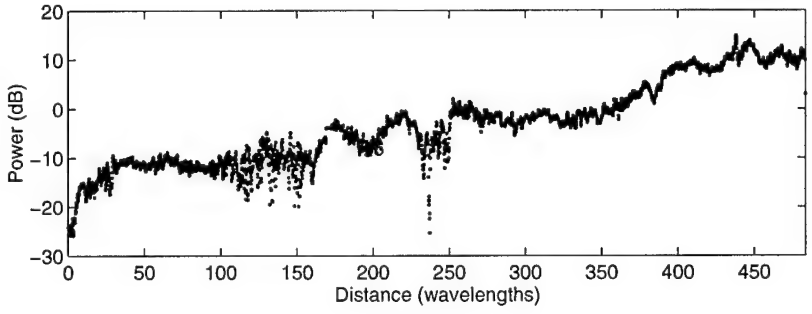

(c)

Figure 7: Measurements taken on April 19 showing (a) a map of the transmitter route, (b) the estimated bearing, and (c) the received signal power (averaged for all channels).

bearing results. This polynomial was then used to compute the "true bearings". This also removes errors due to multipath at the receiver site, equalization errors, and mutual coupling effects. The result is plotted in Figure 8.

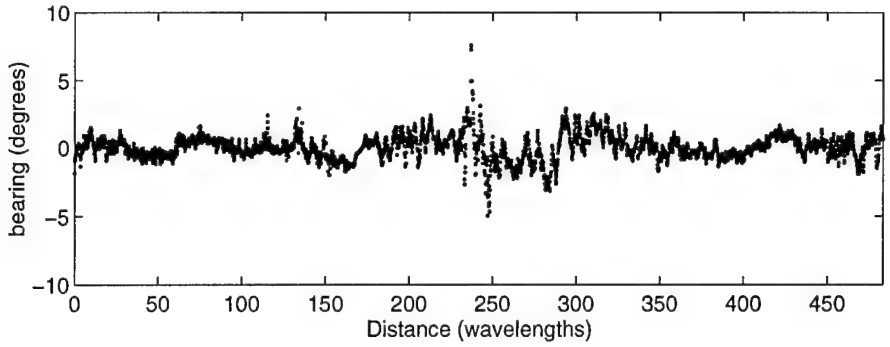

Figure 8: Bearing error difference between DF estimates and smoothed DF estimates calculated using a ninth order polynomial model.

Upon examination, it is apparent that multipath effects are prevalent everywhere on the DREO site although some locations are worse than others with peak to peak errors up to 5° or more. Based on Figure 8 the RMS bearing error for a transmitter on the DREO site was 1.3° or greater.

3.4 May 5

On May 5, two experiments were performed using the same procedure used on April 8 and 12. The location of the transmitter routes are shown in Figure 9a. Together they formed a single continuous route which overlapped half of the route used on April 8. The joint results are shown in Figure 9b and c and have been aligned as if the transmitter followed a single route encompassed by the arrows marked 8 and 9 in Figure 9 (in this case transmitter distances are measured with respect to the starting position for measurement set 8). The results for measurement sets 7 and 10 have been offset downwards.

The results provide further support for the conclusions drawn from the previous experiments. Additionally, comparing the bearing results shown in Figure 10 for the overlapping measurements taken on April 8 and May 5 (offset 2° downwards) indicates that, at least during the one month period between measurements, the multipath environment had not changed significantly. In fact, the agreement between measurements was sufficiently close that aligning the bearing error patterns was used to make minor corrections to improve the estimated positions of the transmitter vehicle on May 5.

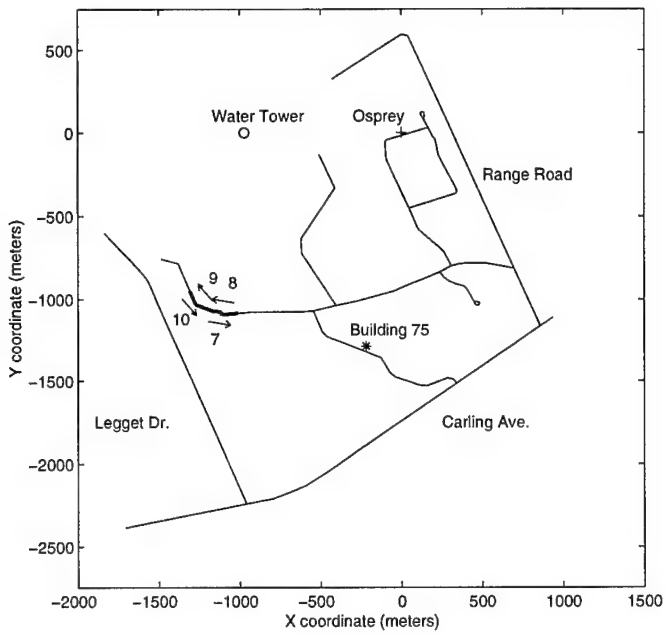

(a)

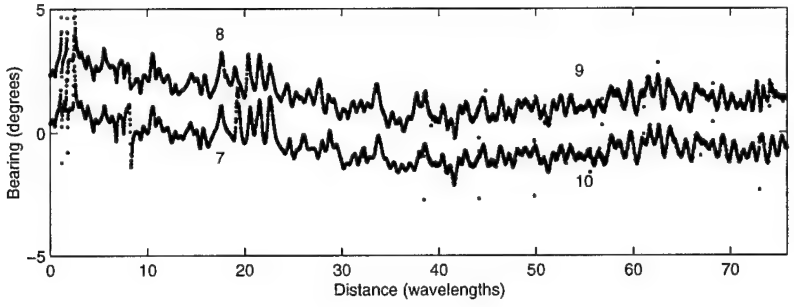

(b)

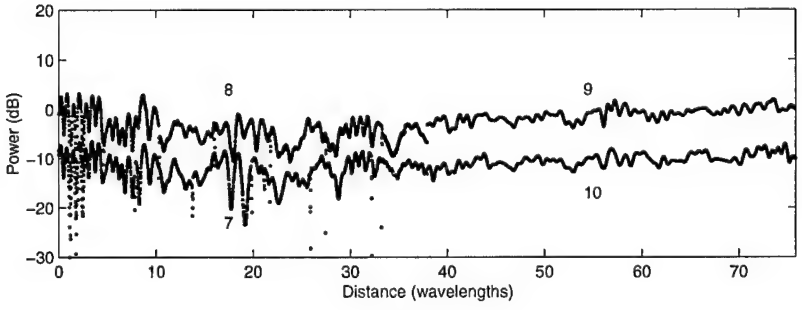

(c)

Figure 9: Measurements taken on May 5 showing (a) a map of the transmitter route, (b) the bearing errors, and (c) the received signal power (averaged for all channels).

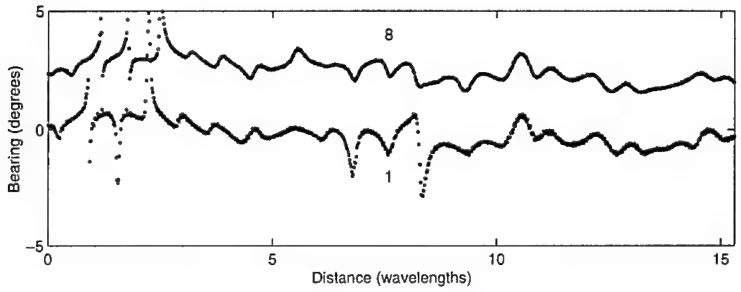

(a)

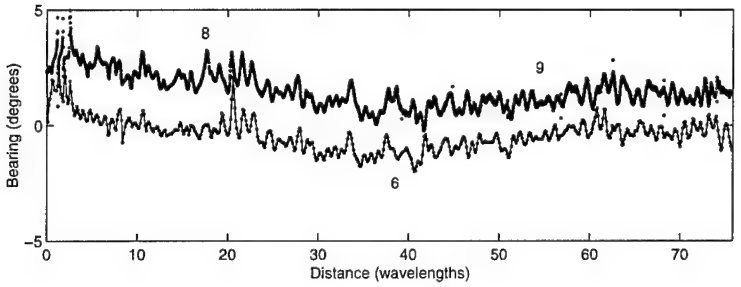

(b)

Figure 10: Comparison of bearing errors from May 5 (measurement sets 8 and 9) with bearings errors from (a) April 8 (measurement set 1) and (b) May 5 (measurement set 6).

3.5 May 16

As was done on May 5, experiments were paired in order to effectively double the distance travelled by the transmitter. However, in this case the reverse path was not measured since, based on the repeatability of the results from the previous experiments, this did not appear to be necessary. Additionally, two different double paths were measured as shown in Figure 11a. The paths were chosen to be at different ranges but covering the same bearings. The results are shown in Figure 11b and c. In this case the results have been plotted as a function of the map bearing instead of distance travelled by the transmitter. As has been done previously, for ease of comparison the results for measurement sets 13 and 14 have been offset downwards (2° in Figure 11b and 10 dB in Figure 11c).

Comparing the results from the two different ranges, the longer variations appear to correlate, but there are definite differences in the fine structure. This has serious consequences for on-site antenna array calibration of a DF system because it suggests that the normal procedure for measuring the antenna array manifold at a given frequency (i.e. using a target transmitter which changes in azimuth but is fixed in range) will achieve only limited success – the calibration would have to be performed as a function of range as well as azimuth to achieve high accuracy ($< 0.1°$).

3.6 May 18

On May 18, the transmitter antenna was mounted on the transmitter vehicle and the vehicle driven slowly down Riddell Road (as shown in Figure 12a) while measurements were taken with the Osprey system. The total route travelled was 1.9 km and transmission was terminated prematurely due transmitter equipment problems. Vehicle speed was approximately 7-8 kph. Elapsed time was noted every 0.5 km from the starting position measured using the vehicle odometer. The times that landmarks shown on the map were passed was also recorded. Based on these known positions versus times, other transmitter positions could be interpolated for all other times then correlated with the DF measurements. The results are shown in Figure 12b and c. Note that in Figure 12b the slower variations in the bearing error results (as a function of distance travelled) may have been partly due to uncertainty in the vehicle position.

The main purpose of this experiment was to determine whether the multipath effects

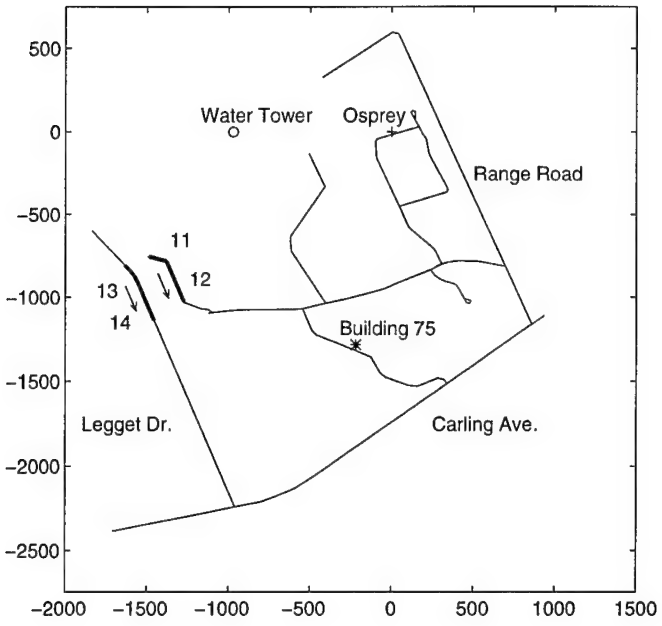

(a)

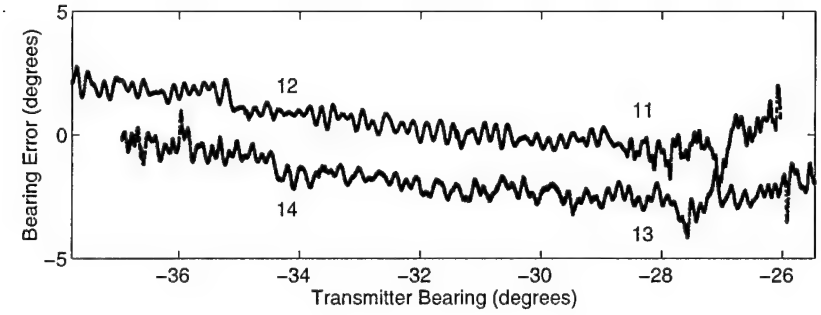

(b)

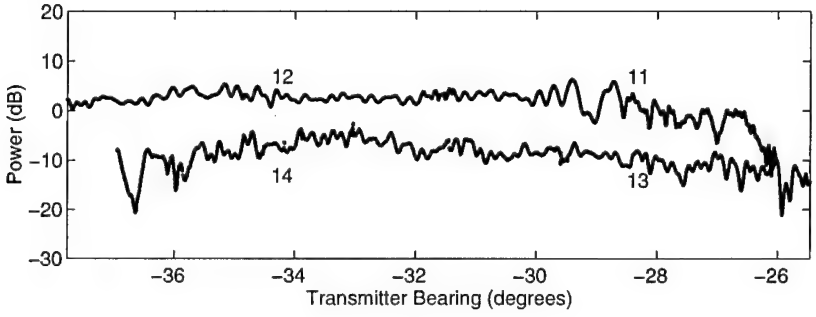

(c)

Figure 11: Measurements taken on May 16 showing (a) a map of the transmitter route, (b) the bearing errors, and (c) the received signal power (averaged for all channels).

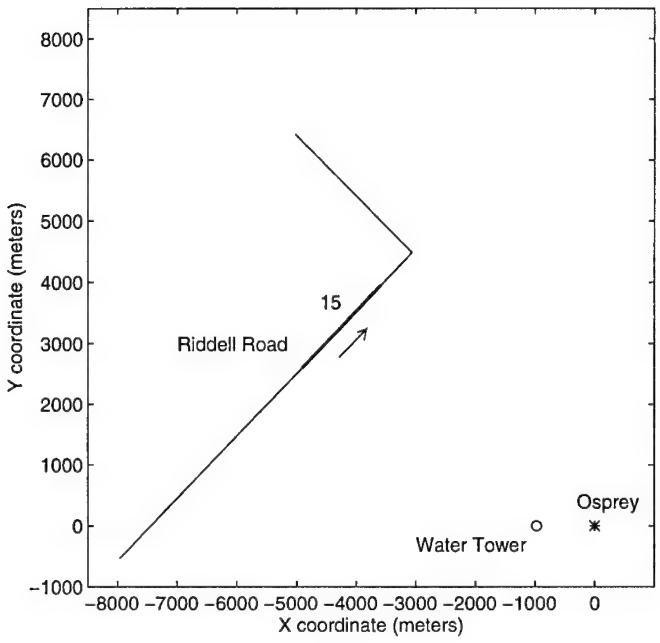

(a)

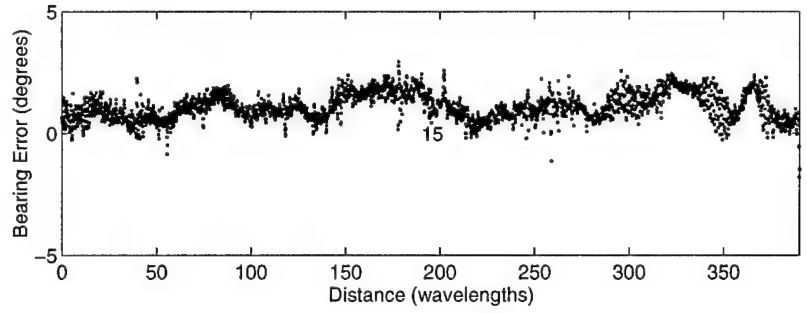

(b)

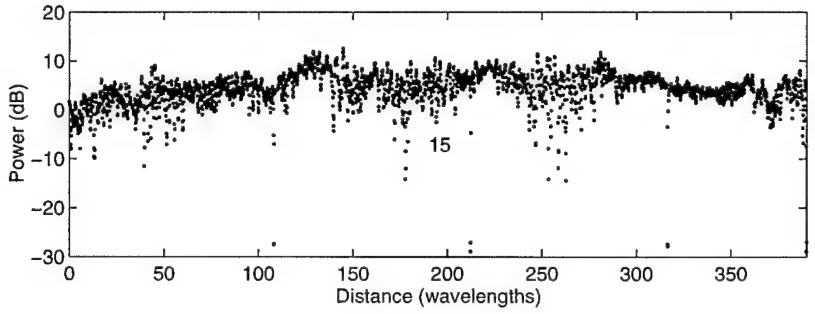

(c)

Figure 12: Measurements taken on May 18 showing (a) a map of the transmitter route, (b) the bearing errors, and (c) the received signal power (averaged for all channels).

(i.e. the rapid fluctuations in bearing error as a function of transmitter position) observed at ranges under 2 km also occur at greater ranges (5 km). From the results shown in Figure 12b and c, the answer would appear to be "yes". A blow-up of the bearing error for distances travelled from 38λ to 58λ confirms this conclusion with rapid fluctuations on the order of 1λ clearly evident in the data shown in Figure 13a. Since the received signal power levels during this experiment were lower than previous experiments (i.e. lower SNR), the transmitter was measured while stationary to determine the significance (if any) of temporal effects. The corresponding bearing results are shown in Figure 13b. The length of time shown corresponds to the length of time required to make the measurements in Figure 13a. Although temporal noise clearly affected the results, multipath was still the dominant factor.

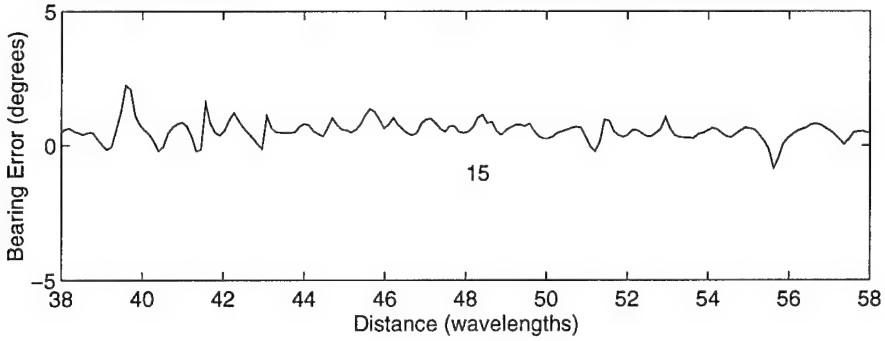

(a)

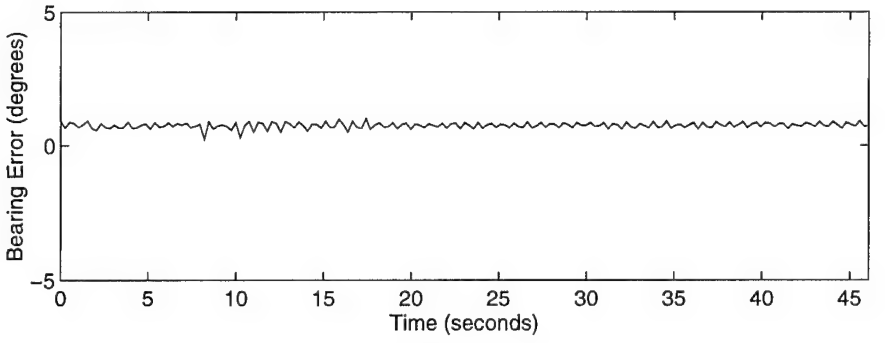

(b)

Figure 13: Blow-up of May 16 bearing errors showing (a) error for moving transmitter, and (b) error for stationary transmitter.

3.7 May 27

On May 27, the procedure first employed on April 8 was again used. The route followed is shown in Figure 14a. Originally measurements were taken as the transmitter was moved in both directions (north and south). Difficulties in maintaining the transmitter antenna upright as the transmitter travelled in the southern direction resulted in the corresponding measurement set being discarded. (The problem was a result of the fact that part of the route was on a field with long grass which did not provide a stable platform for the antenna). The bearing error and received power results are shown in Figure 14b and c.

The main purpose of this experiment was to determine whether the multipath effects (rapid fluctuations of the bearing error as a function of transmitter position) observed at longer ranges (1-5 km) occur at shorter ranges. Clearly they do.

A second purpose was to determine whether the bearing errors at short ranges correlated. To check this, the bearing error results from measurement sets 7, 9, 11 and 12 were merged and plotted as a function of actual transmitter bearing in Figure 15. These results are shown offset downwards by two degrees. The bearing error results from May 27 for the same bearing interval are also shown in the same plot. Comparing the results there appears to be little correlation between the short range and longer range results except, perhaps, the gradual downwards trend in bearing error.

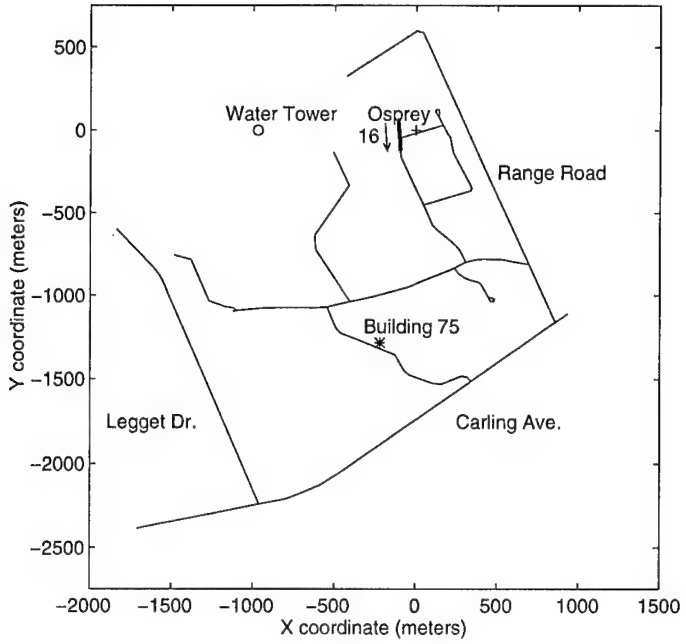

(a)

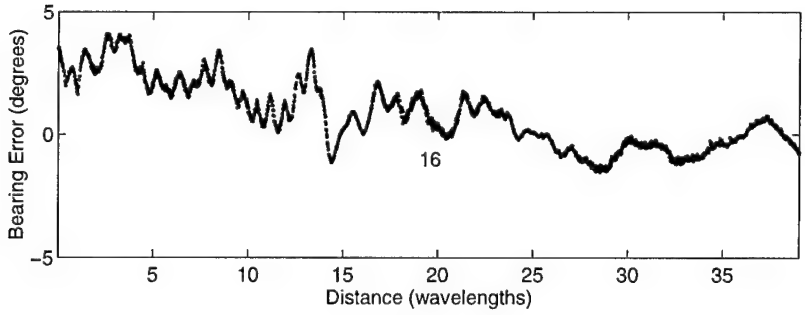

(b)

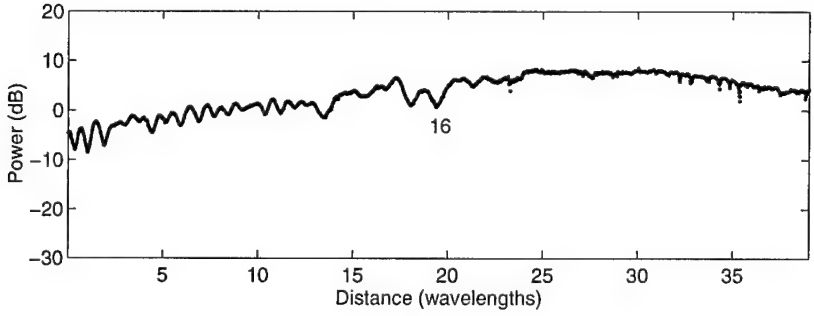

(c)

Figure 14: Measurements taken on May 27 showing (a) a map of the transmitter route, (b) the bearing errors, and (c) the received signal power (averaged for all channels).

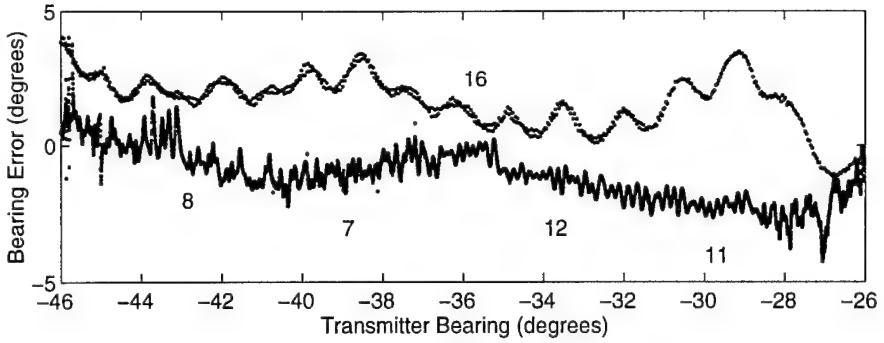

Figure 15: Comparison of bearing error results for May 27 (measurement set 16) with the merged bearing error results from May 5 and May 16 (measurement sets 7, 9, 11, and 12).

3.8 May 30

The experiment on May 30 was a repeat of May 18, except that the transmitter was measured over a much longer route which included rounding a corner and travelling in a direction almost directly away from the Osprey system as shown in Figure 16a. To provide better position accuracy, the transmitter frequency was changed 10 Hz for approximately 2 second every 0.1 km (according to the vehicle odometer) to mark the position in the recorded data. This results in position errors of up to ± 50 meters which corresponds to errors in the map bearings of $\pm 0.5°$. The measurement bearing errors and power results are shown Figure 16b and c.

As in the short range case, the rapid variations in the data are still apparent in the bearing and amplitude results although the scatter in these results decreased once the transmitter rounded the corner (at 350λ) and headed away from the receiver. Quantitatively, the RMS bearing error was 1.7° for measurement set 17 and 0.6° for measurement set 18.

Measurement set 18, beginning at 350λ in Figure 16, is particularly interesting from the DF antenna array calibration point-of-view. This was the only case where the transmitter was moving on a route almost directly in line with the receiver so that only the multipath environment around the transmitter was significantly changing. Assuming that most of the mean bearing error is due to multipath sources near the DF receiver, the standard deviation of the bearing errors then gives an estimate of the RMS error contribution due to multipath sources near the transmitter. The standard deviation for this case was 0.3°. Hence, even if on-site antenna array calibration could compensate for the bearing errors due to multipath sources near the DF receiver, bearing errors due to multipath

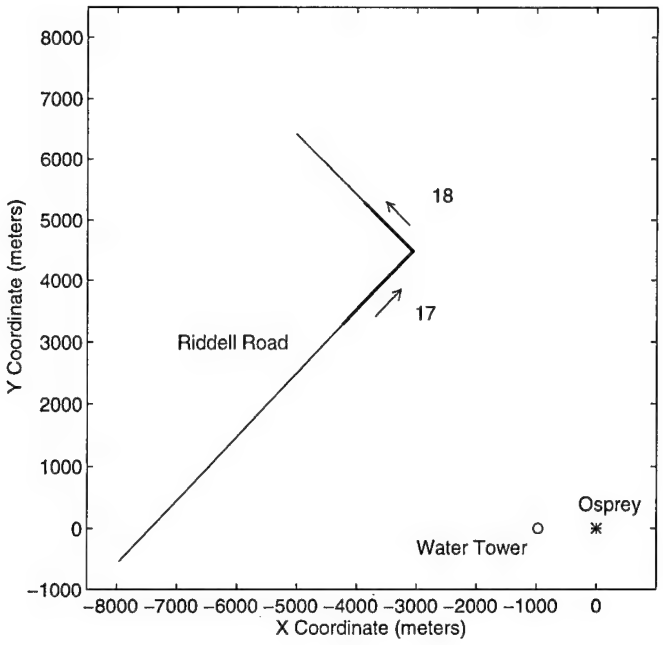

(a)

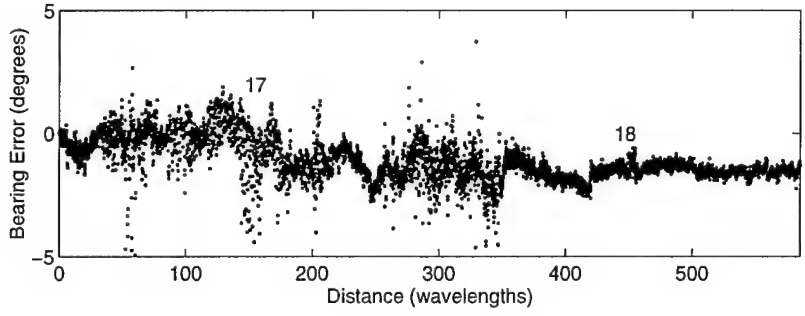

(b)

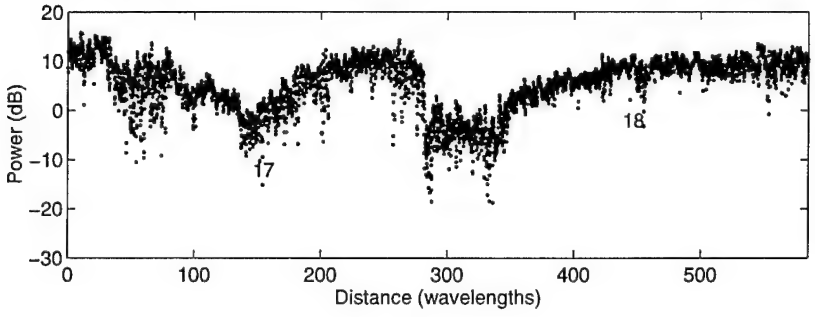

(c)

Figure 16: Measurements taken on May 30 showing (a) a map of the transmitter route, (b) the bearing errors, and (c) the received signal power (averaged for all channels).

sources near the transmitter would still be greater than desired (i.e. $> 0.1°$). This is consistent with the conclusion drawn from a comparison of measurement sets 11 and 12 with measurements sets 13 and 14 in Section 3.5.

4.0 SPATIAL FREQUENCY ANALYSIS

In the previous section, ripple effects were observed in the bearing and power measurements which were attributed to multipath propagation. In this section, a more detailed analysis of these effects is presented beginning with the theory for a single multipath source. Based on this theory, it is then shown that the spatial frequency of the ripple observed in the data provides useful information about the location of the multipath source. Finally, given the usefulness of the spatial frequency information, the ripple analysis is extended to the case of multiple sources of multipath using the Fourier transform – an approach which becomes particularly useful in Section 5 when comparing simulation data with the field trial data.

4.1 Ripple Effects

The observed ripple in the bearing and power measurements is a direct consequence of multipath propagation. It is due to the difference between the change in path length of the direct signal path with respect to all the secondary signal paths as the transmitter moves. For example, consider the simple case of a single multipath source as shown in Figure 17. The signal picked up by the receive antenna is the summation of the direct and a secondary signal. The amplitude of the received signal will be dependent on both the amplitude of the component signals as well as their relative phases. Amplitude and phase are, in turn, functions of the lengths of the signal paths. Since the transmitter is located some distance from the receiver, when the transmitter moves from the first position to the second position, the changes in path lengths for the direct and secondary signals will be relatively small compared to the total paths. The corresponding change in amplitudes of the component signals will be small and noncyclical, so it is obvious that amplitude effects alone cannot explain the ripple observed in the measurements. On the other hand, if the path length difference between the direct and secondary signal changes a distance as small as one wavelength, the two component signals cycle through both in-phase and out-of-phase conditions resulting in very pronounced changes in the received signal amplitude as the transmitter moves. Obviously if the transmitter moves further, this behaviour will repeat over and over which is consistent with the ripple effects observed in the measurement data.

The spatial frequency of this ripple (i.e. the frequency of the ripple measured as a function of transmitter distance travelled) will be dependent on how quickly the direct

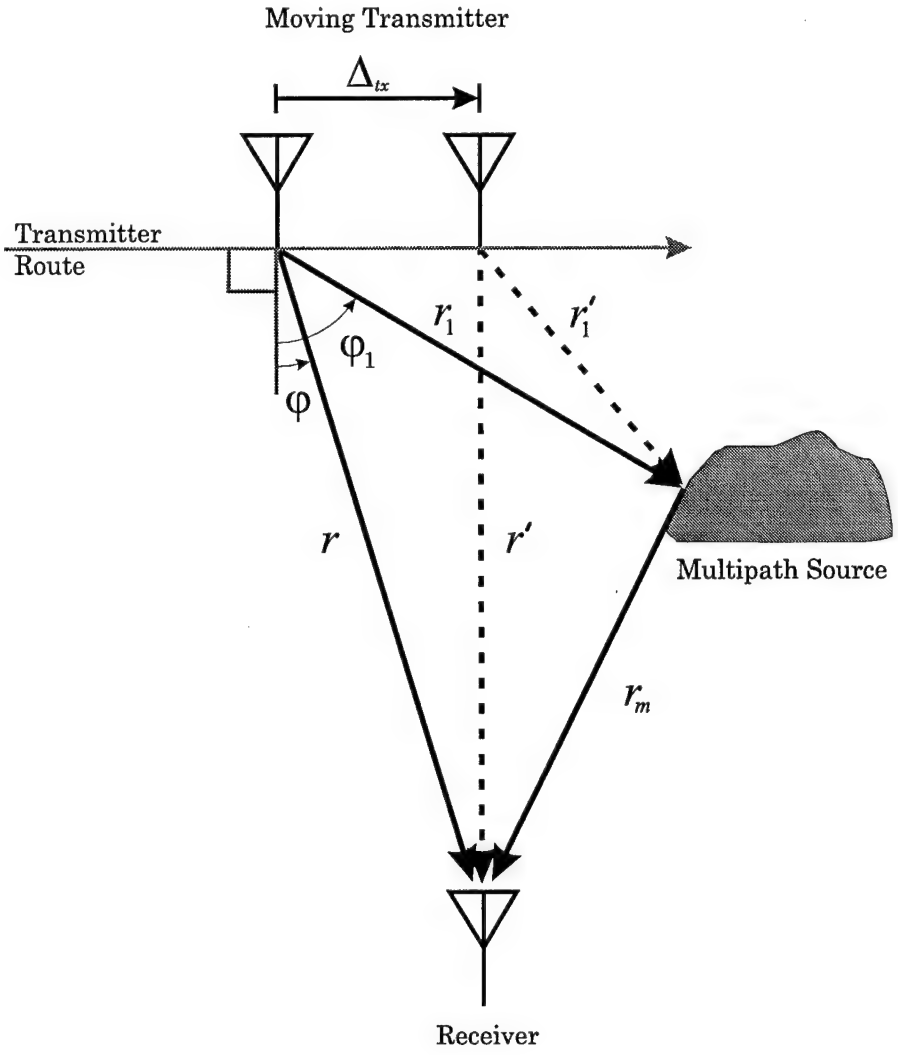

Figure 17: Example of the generation of ripple in the measurements due to multipath.

and secondary path difference changes as the transmitter moves. This can be derived mathematically using Figure 17 as a guide. To begin with, the differential path length is given by

$$l = r_1 + r_m - r \tag{1}$$

for the first position, and

$$l' = r_1' + r_m - r' \tag{2}$$

for the second position. The change in path length difference between these two transmitter positions is given by

$$l' - l \;=\; (r_1' + r_m - r') - (r_1 + r_m - r) \;=\; (r_1' - r_1) - (r' - r) \tag{3}$$

Letting Δ_{tx} represent the distance travelled by the transmitter, then r' can be defined in terms of r as

$$r' \;=\; \sqrt{r^2 + \Delta_{tx}^2 - 2r\Delta_{tx}\sin\varphi} \;\approx\; r - \Delta_{tx}\sin\varphi \tag{4}$$

where it is assumed $r \gg \Delta_{tx}$. Similarly

$$r_1' \;=\; \sqrt{r_1^2 + \Delta^2 - 2r_1\Delta\sin\varphi_1} \;\approx\; r_1 - \Delta_{tx}\sin\varphi_1 \tag{5}$$

The direction angles φ and φ_1 (shown in Figure 17) are similar in definition to bearing angles except they are measured perpendicular to the transmitter route instead of perpendicular to the receiver baseline. Using these relationships to simplify (2),

$$l' - l = \Delta_{tx}(\sin\varphi_1 - \sin\varphi) \tag{6}$$

The average spatial frequency for the transmitter distance moved can now be defined as

$$f_s \;=\; \left|\frac{l' - l}{\Delta_{tx}}\right| \;=\; |\sin\varphi_1 - \sin\varphi| \tag{7}$$

where the spatial frequency can be interpreted as the number of times the phase difference between the direct and secondary path cycles through 360° as the transmitter is moved over a distance of one wavelength, i.e. f_s is measured in terms of cycles per wavelength (abbreviated to cpw in this report).

4.2 Localizing Multipath Sources

For a given spatial frequency, equation (7) can be used as a guide to the location of a multipath source. For example, the contour lines in Figure 18 show the possible locations of a multipath source for a given spatial frequency. The transmitter-receiver geometry is the same as used for measurement set 12.

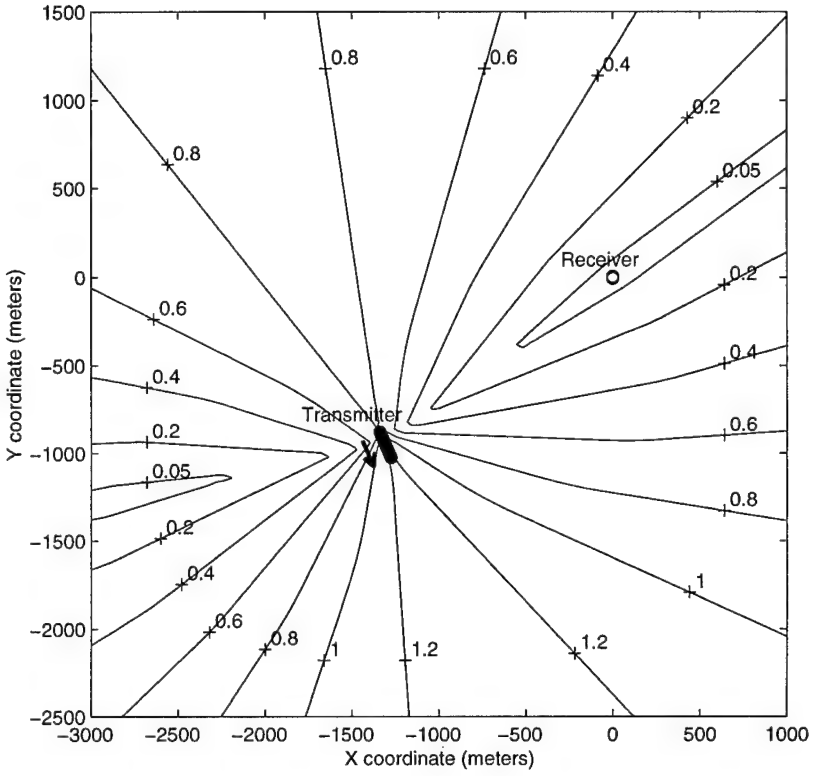

Figure 18: An example of spatial frequency generation as a function of multipath source position.

A few observations based on both equation (7) and Figure 18 are in order here. The highest spatial frequencies occur when the transmitter moves directly towards/away from the multipath source ($\varphi_1 = \pm 90°$) and further from/closer to the receiver. In the example, the multipath source locations lining up with the transmitter route in the forward direction of travel give rise to the highest spatial frequencies (1.26 cpw).

The highest possible spatial frequency $f_s = 2$ cpw occurs for the geometry where the line of travel of the transmitter aligns with both the receiver and multipath source ($\varphi = -\varphi_1 = \pm 90°$), i.e. the transmitter moves directly towards/away from the receiver and directly away from/towards the multipath source. At this frequency the relative

phase cycles through 360° every one half wavelength travelled by the transmitter.

The lowest spatial frequencies occur for multipath sources located along the line of the direct signal path, i.e. the direction angle $\varphi = \varphi_1$ resulting in $f_s = 0$ cpw. Additionally, for multipath sources located near the receiver $\varphi \approx \varphi_i$, so that the generated spatial frequencies will also be low. These effects are illustrated in Figure 18, except that along the direct signal path near the transmitter $f_s \neq 0$. This is due to the fact that since the transmitter is moving, the condition $\varphi = \varphi_1$ and $f_s = 0$ occurs only momentarily for one transmitter position, so that for the other transmitter positions $f_s > 0$ (only the highest value is actually plotted).

4.3 Multiple Multipath Sources

In the real world, many sources of multipath exist, so that the ripple generated in the measured data will be a combination of many frequencies. To isolate the various frequency components, a discrete Fourier transform (with respect to transmitter displacement) can be performed on the data. Performing a discrete Fourier transform on the power measurements from measurement set 12, and appropriately scaling, yields the results shown in Figure 19.

The main features of the frequency spectrum include the large peak at 0 cpw due to the direct signal, multipath sources near the receiver, and measurement errors. The plateau from 0.1 to 1.1 cpw is predominantly due to multipath sources near the transmitter. Above 1.26 cpw (the maximum predicted frequency value for this case), the power level is considerably lower. This residual power is produced by temporal noise and intermodulation products caused by the inherent nonlinearities in generating the power results (i.e. computing the power involves squaring the IQ data). The lack of multipath power between 1.15 and 1.26 cpw is most likely due to the fact that these frequencies correspond to locations on or very close to the road – locations which were free of any obvious obstacles.

The results shown in Figure 19 provide strong support for the explanation given for the generation of the ripple. The results also indicate, although not conclusively, that multipath is generated from many directions around the transmitter resulting in the plateau in Figure 19). Finally, evaluating the spatial frequency components in the plateau region provides a means of evaluating sources of multipath in the vicinity of the transmitter, or at least some distance from the receiver. Restricting the analysis to the plateau region is also

useful for removing the effects of measurement errors due to mutual coupling, improper antenna array equalization, instrumentation biases, and some temporal noise. This approach to processing the measurement data is used to advantage in the next section when the problem of identifying the most appropriate multipath source model is considered.

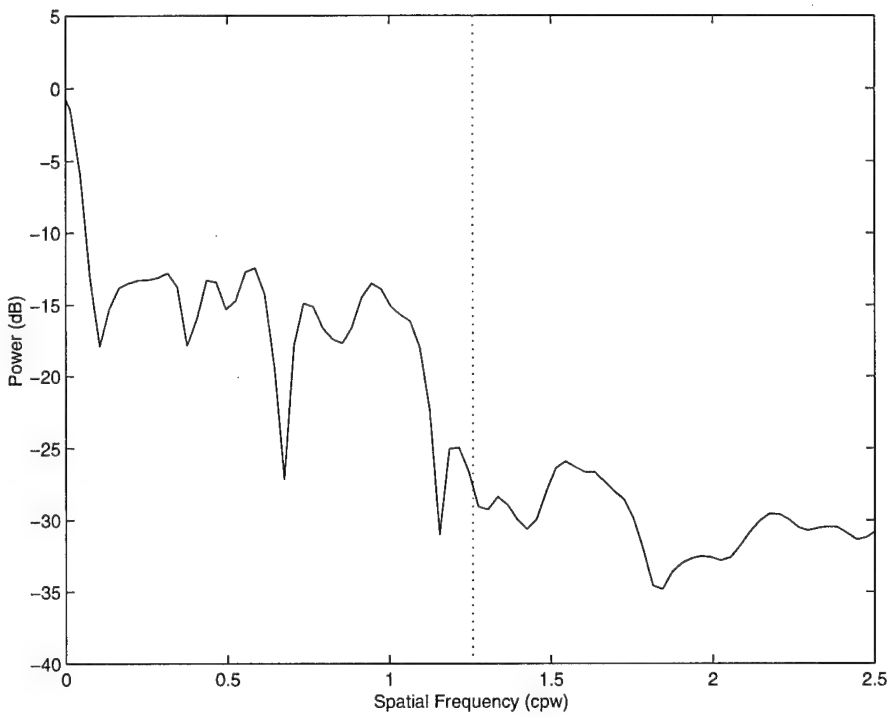

Figure 19: Spatial power spectrum of the power measurements from measurement set 12. The dotted line shows the maximum predicted value of 1.26 cpw.

One final comment; the dependency of the ripple frequency on the direction angles φ and φ_1 raises the interesting possibility of localizing the sources of multipath and deriving information about the environment this way. For example, using the discrete Fourier transform to determine the spatial frequency components, the corresponding angle φ_1 could easily be determined by rearranging (7) given that φ is known. The corresponding multipath source bearing ϕ_m could also be computed by taking advantage of the spatial diversity of the receiver array. Unfortunately, attempts to implement this approach have met with only limited success. The main difficulty is that the spatial frequency attributable to any one multipath source changes as the transmitter moves, and the way it changes is a function of geometry. If there are too many multipath sources, which there appeared to be when the field trial measurement data was analyzed, it becomes too difficult to accurately separate the individual multipath components in the spatial frequency domain using the discrete Fourier transform. Wavelet transform techniques might offer a

solution to this problem, however, this avenue was not pursued.

5.0 MULTIPATH MODELLING

In the previous section, spatial frequency analysis was shown to provide useful information on the amount of multipath present and the locations of the sources. However, this information is approximate at best. To sharpen these estimates, a computer simulation approach is employed, which, when coupled with the spatial frequency approach, reveals much more information about the multipath environment and its effects.

In the following discussion, various shapes and sizes of multipath sources are investigated. Simulations are then described which incorporate a large number of these multipath sources. Based on the simulated measurements, a method to differentiate between the various models is developed. This method is then applied to the field measurements to determine and then refine the multipath model which is the most appropriate. Using the refined model as a guide, the dominant sources of multipath generated in the field measurements are identified and estimates of the number of sources and their distribution are also made.

5.1 Simulation Description

The actual computer modelling approach used is described in detail in [2]. Essentially, for modelling purposes the ground is taken to be either: (a) a perfectly reflecting plain with sources of multipath lying on top of it (including terrain features and vegetation); or (b) a reflecting plain interspersed with patches which are not perfectly reflecting (i.e. modelling changes in the electrical properties of the ground). In either case, the path losses are markedly similar, except for the addition of a height coefficient for the terrain/vegetation model. Since multipath power rapidly increases with elevation, and since vegetation and terrain were a prominent feature of all the signal paths measured, only terrain and vegetation effects are modelled in this report.

For the simulations, each individual multipath source was modelled as a collection of discrete isotropic reradiators. Initially, only four very different multipath sources were considered as shown in Figure 20. These four multipath sources were: (a) a small hemisphere with a diameter of 2 meters used to represent the scattering effects of small objects such as bushes, rocks, etc.; (b) a lollipop shape with the dimensions of a typical deciduous tree which gives rise to some diffraction and shadowing effects; (c) a hemispherical shape

representing a mound or small hill and, from its size, having a more pronounced shadowing effect than the smaller objects; and (d) a wall-like object which might represent the side of a building where the flat surface acts as a good reflector.

To simulate the real world measurements, the set up shown in Figure 21 was used to duplicate the transmitter-receiver geometry of measurement set 12 (see Figure 11a). A large number of multipath sources were also randomly and uniformly placed over the entire area. For any particular simulation, the multipath sources were all identical, and chosen as one of the four shown in Figure 20. In simulations using the wall-like reflector model, the wall surface of each multipath source was chosen to be vertical with the lowest edge parallel to the ground plane and randomly aligned in azimuth.

To ease the computational requirements, the received multipath signals were calculated ignoring the coupling effects between multipath sources (the *internal coupling* approach described in [2]). When coupling is ignored, the main error is an overestimation of the received multipath power since the effect of multipath sources shadowing other multipath sources is not accounted for. This problem obviously gets worse as the density of multipath sources increases. Hence, to maintain an acceptable level of error, multipath sources were not placed closer than the distance D^2/λ (where D is the largest dimension of the multipath source) to each other, the transmitter, or the receiver.

An obvious problem with this minimum spacing restriction is the fact that in real life there is no such restriction. This does not pose serious difficulties, however, since two or more objects close enough to strongly couple could be modelled as a single object, e.g. a group of trees would be modelled as a single grove.

To provide a small statistical data base for comparison purposes, 50 simulations were run using each model for a total of 200 simulations. The densities of multipath sources were chosen to produce direct signal to multipath power ratios in the range of 10-20 dB. In each simulation, the transmitter was moved one meter at a time, and for each position a measurement of the amplitude and phase of the received signal was made.

Examples of the simulated received power and DF results for each multipath model are shown in Figures 22 and 23. It is evident by comparing the simulated results with the results from measurement set 12 that the multipath power levels were too low to produce the equivalent ripple in both DF error and power. Multipath power can be increased by increasing the density of multipath sources and decreasing the spacing requirement, but this comes at the expense of decreased accuracy due to the fact that coupling effects are

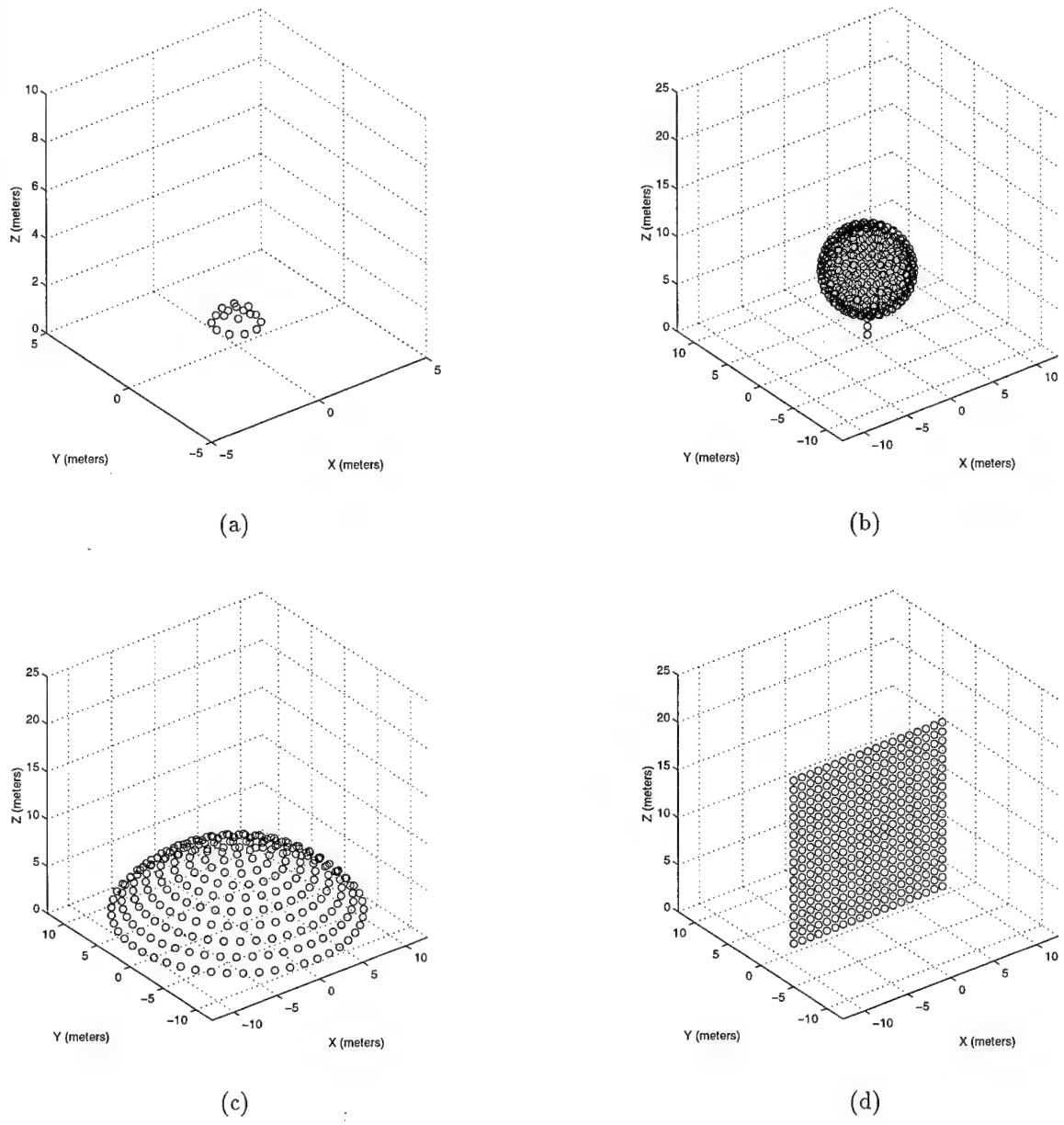

Figure 20: Shape of multipath sources showing reradiator positions for (a) small scatterer model, (b) tree model, (c) hill model, and (d) large reflector model.

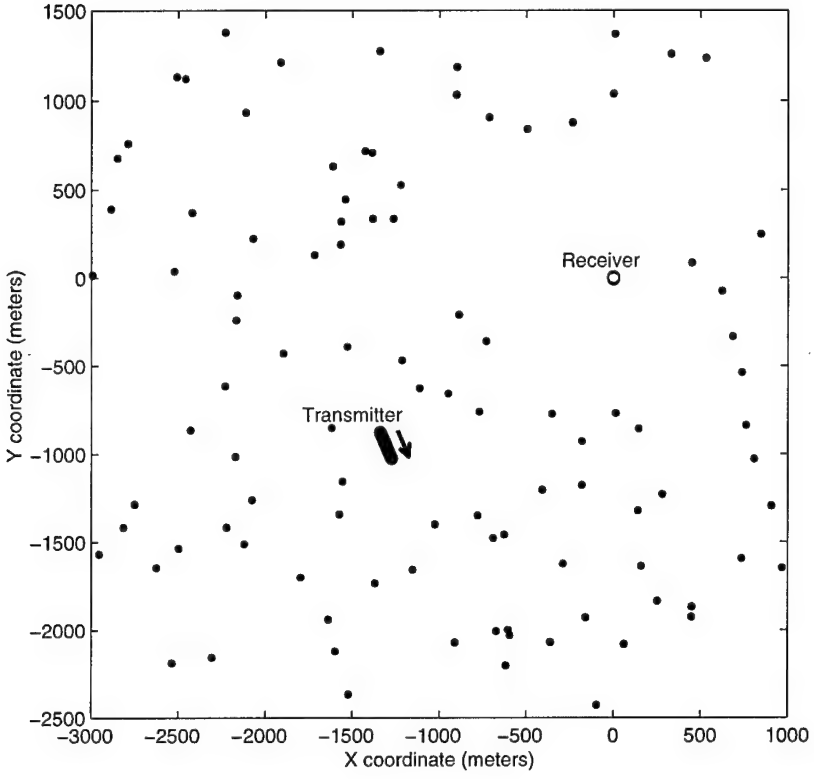

Figure 21: Map of setup used for simulation examples.

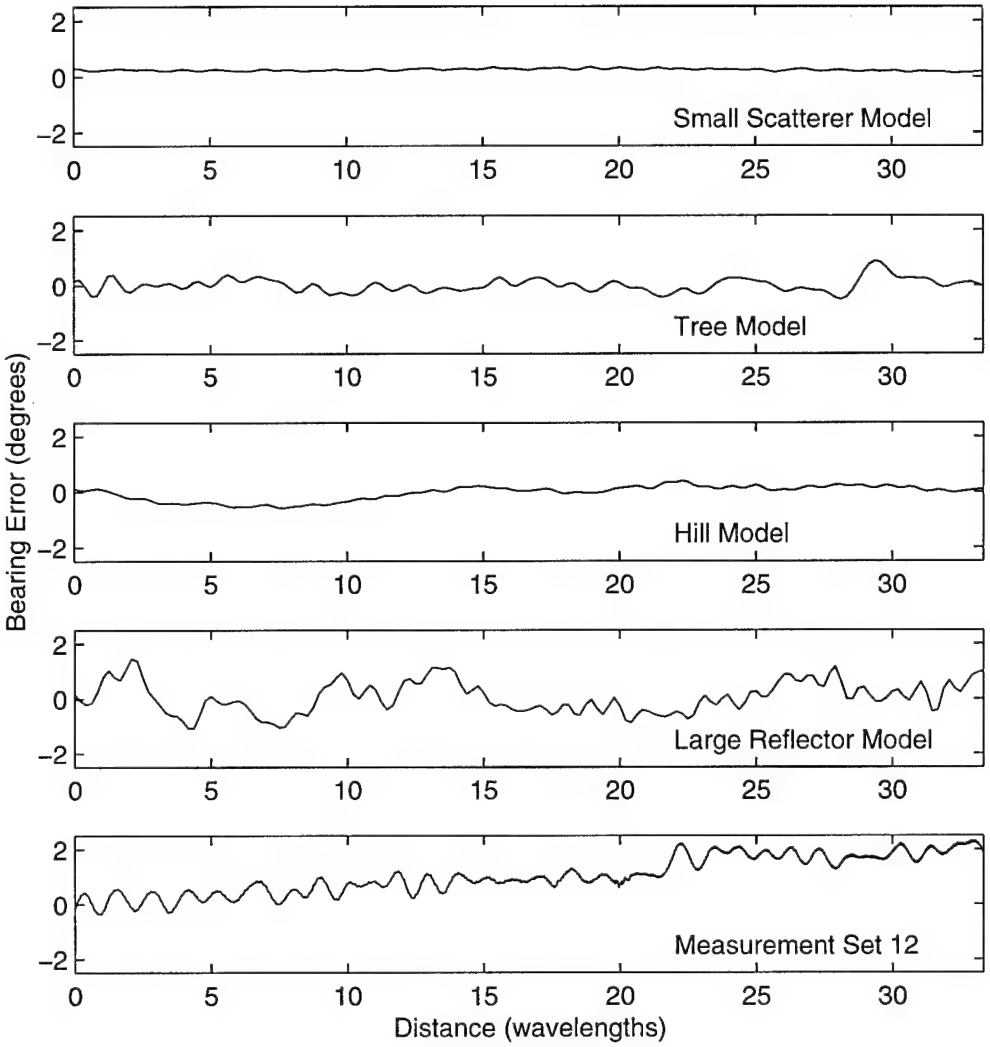

Figure 22: Bearing error results showing one example from each of the four simulation sets. The results for measurement set 12 have also been shown for comparison.

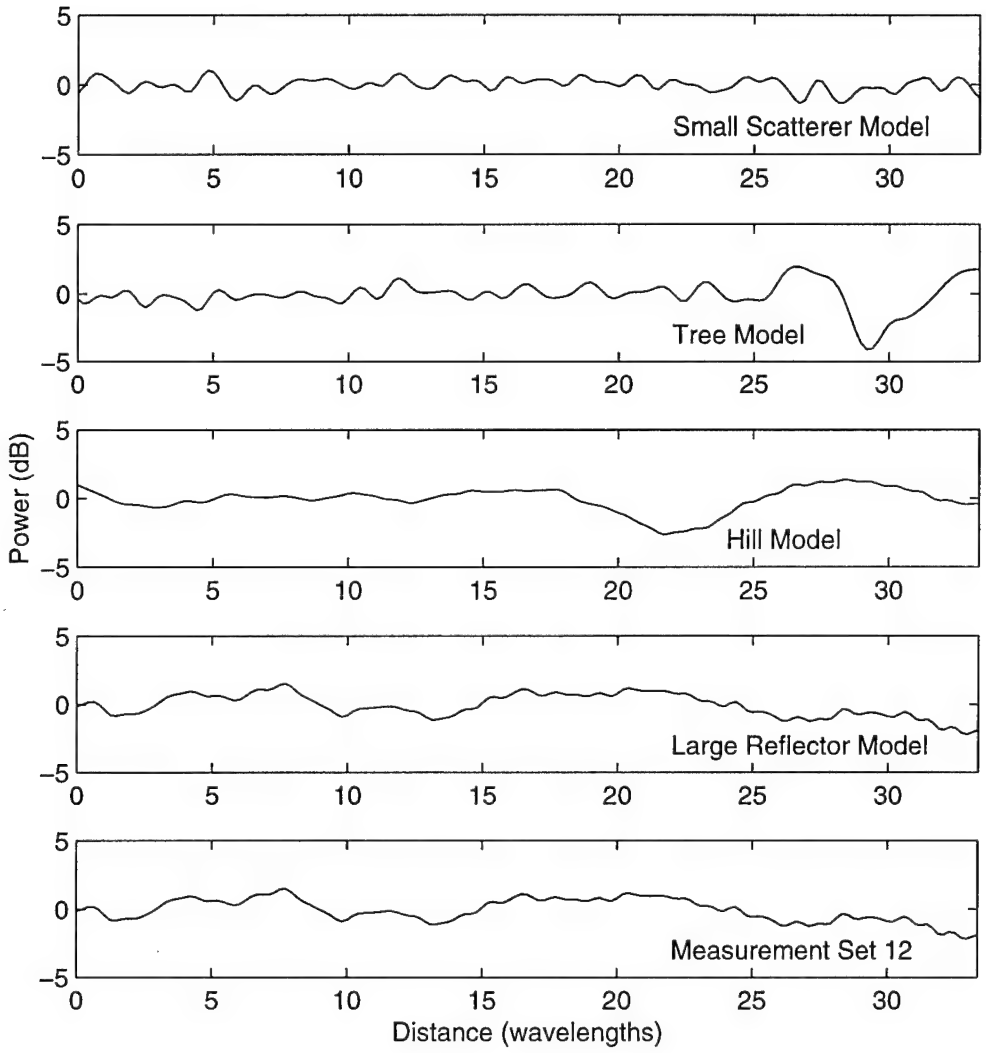

Figure 23: Received power results showing one example from each of the four simulation sets. The results for measurement set 12 have also been shown for comparison.

ignored. Fortunately, other features of the real and simulated data can be compared, yielding useful information.

5.2 Multipath Regions

A big advantage of simulations is that measurements can be made which would not ordinarily be possible in real life. One such measurement is the measurement of the individual power contribution of each multipath source. This can then be used to assess where the significant multipath sources are located.

Figure 24a-d contains maps showing the location of the most significant multipath sources based on a single simulation of each model. In this case, the most significant multipath sources were considered to be those which contributed 99.9% of the total multipath power. For simplicity, the areas containing these significant sources are called the multipath regions. The choice of 99.9% as a cutoff value is somewhat arbitrary, but provides a means of assessing the shape of the multipath region regardless of the density of multipath sources. Later on, as a more refined model is developed, region size and shape will be assessed in a manner relating more directly to bearing error.

The size and shape of each region is controlled by path losses and geometry. For a terrestrial path with the transmitting and receiving antennas near the ground, the path loss is proportional to r^4 where r is the transmitter-receiver path length. For a large reflecting or shadowing type multipath source, assuming the geometry is favourable, the multipath signal can be modelled as simply being redirected by the multipath source which yields a path loss given by $(r_1 + r_2)^4$. For a small scattering source, the multipath signal can be modelled as a signal first received by the scattering source followed by a retransmission to the receiving antennas. This yields a much higher path loss given by $r_1^4 r_2^4$ where r_1 and r_2 represent the transmitter-multipath source and the multipath source-receiver path lengths respectively. The higher the path loss, the smaller the region of influence.

In Figure 24a, for example, the high losses incurred by scattering results in a tight clustering of the significant scattering sources around either the transmitter or the receiver. Additionally because of the high path losses involved, a high density of multipath sources is required to produced the desired amount of multipath power.

For the tree-like multipath sources used in Figure 24b, the multipath region expands

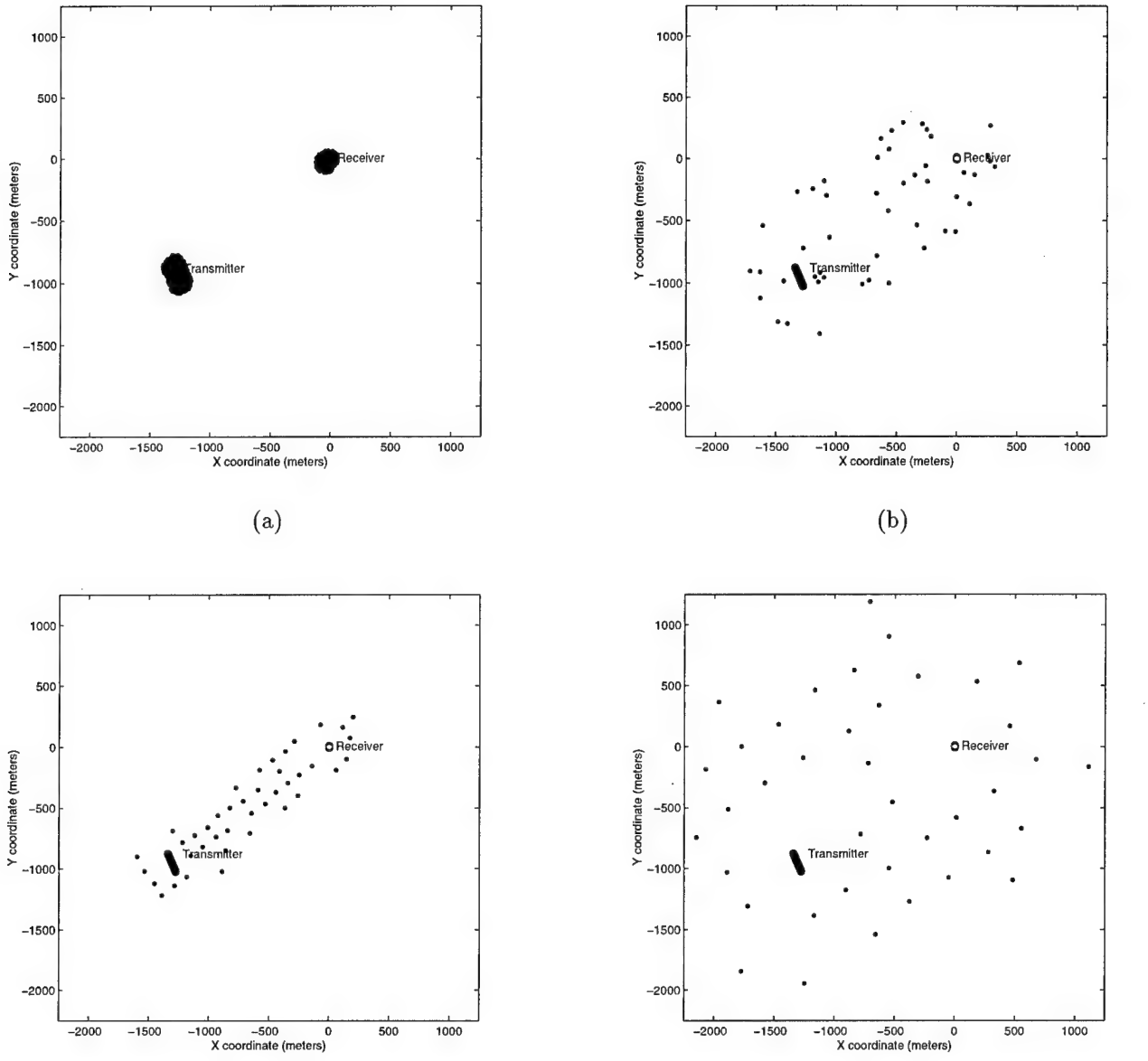

Figure 24: Map of regions containing the most significant sources of multipath for the (a) small scatterer model, (b) tree model. (c) hill model, and (d) large reflector model.

and includes the direct signal path as scattering becomes more directional (i.e. shadowing) and path losses become lower. The density of multipath sources is also lower than for the scattering sources.

For an even larger source, such as the hill-like source used to produce Figure 24c, shadowing effects become more dominant so that the multipath sources along the direct path play a much greater role. As a result, the relative contributions of multipath sources around the transmitter and receiver decrease.

For the large reflector used in Figure 24d, reflection effects become important and the multipath region is greatly increased since favourable orientation of a multipath source can occur anywhere, unlike a shadowing source which is restricted to being close to the signal path. The density of multipath sources in this case is the lowest of all the models.

5.3 Distinguishing Between Multipath Models

The spatial frequency analysis described Section 4.1 can be used in conjunction with the information on multipath region shapes and sizes to try and help identify the kinds of multipath sources that dominate real world measurements. For example, consider the case of measurement 12. If the analysis is restricted to ripple frequencies from 0.4 to 1.26 cpw, the effects of multipath sources located in the exclusion zone shown in Figure 25 are ignored (see also Figure 18). Additionally, if the multipath generation is dominated by sources similar in size to those represented by model 1, then the multipath region surrounding the transmitter will be fairly small as illustrated by the region marked "1" in Figure 25. For multipath generation dominated by sources similar to any of the other models, the multipath region will be larger as also shown in Figure 25.

Defining the diameter of the region as the distance from side to side measured perpendicular to the direct signal path, then the larger the diameter, the greater the bearing range of the multipath sources within the region. Hence, the spatial diversity of a multi-element receive array can be used to provide information about this bearing range, leading to an assessment of the shapes and sizes of the dominant multipath sources.

5.3.1 The Multipath Signal Model

To take advantage of the spatial diversity of the receive array, it is useful to develop

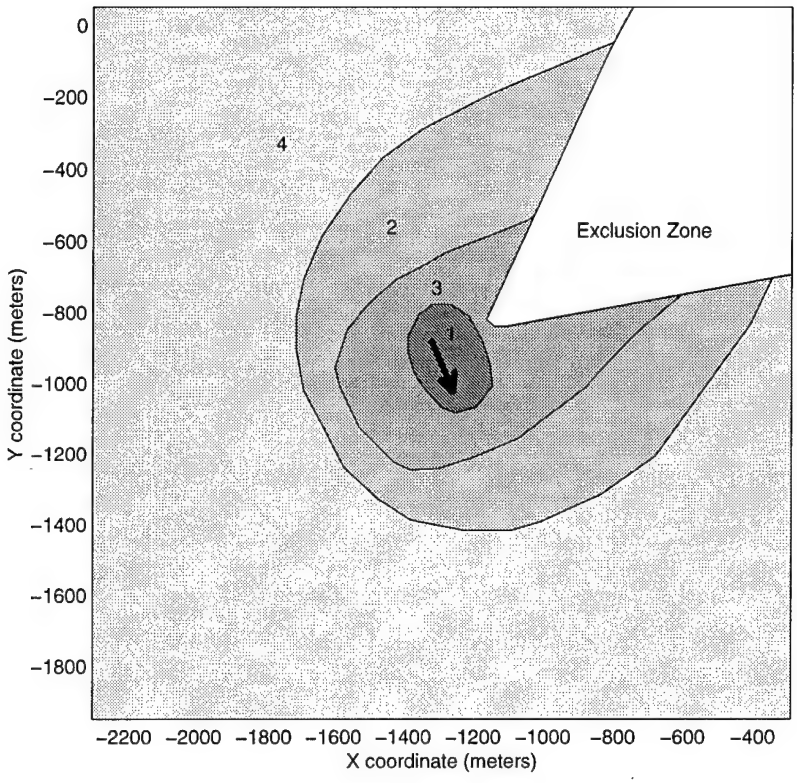

(a)

Figure 25: Map of the area around the transmitter showing the regions containing the most significant multipath sources capable of producing ripple frequencies in the measurement data of 0.4 cpw or more. The numbered zones correspond to the multipath regions that result for the four different multipath models (note that the larger regions include the smaller regions). The black arrow shows the transmitter route.

a mathematical expression of the received signal. Given a uniform linear antenna array with K antennas, M multipath sources, and N sequential transmitter positions uniformly spaced along a straight line, an appropriate expression is given by

$$x_k(d_n) = se^{-j(\frac{2\pi}{\lambda}(r-nd_{tx}\sin\varphi-kd\sin\phi)+\theta)} + \sum_{i=1}^{M} m_i e^{-j(\frac{2\pi}{\lambda}(r_i-nd_{tx}\sin\varphi_i-kd\sin\phi_i)+\theta)} \tag{8}$$

for $0 \leq k < K$ and $0 \leq n < N$, where $x_k(d_n)$ is the IQ measurement sample for channel k when the transmitter has travelled a distance d_n, s is the complex amplitude of the received direct signal, r is the direct signal path length, d_{tx} is the distance the between successive measurements of the transmitter (and $d_n = nd_{tx}$), d is the spacing between adjacent antennas in the receive array, θ is an unknown phase offset introduced by the receiver, m_i is the complex amplitude of the signal received from multipath source i, r_i is the corresponding secondary path length, and ϕ_i is the corresponding bearing of the multipath source.

The above expression deserves some explanation. Each exponential term represents a separate signal: either the direct signal (the first term), or a secondary signal (the terms in the summation). The phase argument in each exponential contains the unknown offset θ plus the path length component. The unknown phase offset θ is a consequence of the fact that during the field measurements the local oscillator circuits in the transmitter and receiver were not synchronized. The result was that slight frequency mismatches between the transmitter and receiver introduced a phase rotation into the data. Under ideal circumstances the phase rotation would have remained constant allowing θ to be estimated, however in practice this was not the case.

To simplify the path length expressions, the assumption was made that the distance between receiver antenna elements was much smaller than the distances to the transmitter or any of the multipath source ($(K-1)d \ll r, r_1, r_2, ..., r_M$). This leads to the approximation:

$$\Delta_0 = -kd\sin\phi \tag{9}$$

which is the difference in the direct signal path length between receive antenna 0 and receive antenna k. Similarly, the difference in secondary path lengths is given by

$$\Delta_i = -kd\sin\phi_i \quad \text{for } 1 \leq i \leq M \tag{10}$$

Additionally, if the multipath sources are also some distance from the transmitter compared to the transmitter distance travelled, then the following approximations for the

change in path lengths between the initial and n^{th} transmitter positions are also appropriate

$$\Delta_0 = -nd_{tx}\sin\varphi \tag{11}$$

and

$$\Delta_i = -nd_{tx}\sin\varphi_i \quad \text{for } 1 \leq i \leq M \tag{12}$$

The assumptions made here also imply that the changes in direct and secondary path lengths are small compared to the total path lengths so that direct and secondary path losses do not change. In other words, the signal amplitudes $s, m_1, m_2, ..., m_M$ may be considered constant which reduces (8) to a simple summation of complex sinusoids that are functions of d_{tx}.

Given the relatively large distances travelled by the transmitter for many of the measurements, the approximation given by (12) and the approximation of constant signal amplitudes are both unrealistic for multipath sources near the transmitter. However, since the following analysis relies on spatial frequency decomposition of the measurements, the effect of a breakdown in these assumptions is no worse than having to deal with a modulated signal in time-frequency analysis instead of a CW signal. Additionally, since the following analysis also relies on comparing simulated and real-world results, as long as the measurements are all processed in the same manner, the breakdown in these assumptions does not pose the difficulties they would otherwise.

5.3.2 Multipath Phase Spread

Based on using (8) to approximate the multipath signal, the next step is to consider a single multipath term from this expression, namely,

$$m_i e^{-j\frac{2\pi}{\lambda}(r_i - r - d_{tx}(\sin\varphi_i - \sin\varphi) - kd(\sin\phi_i - \sin\phi))} \tag{13}$$

Ideally, if this quantity could be determined for all values of i, then the range of variations in the phase of the term $kd(\sin\phi_i - \sin\phi)$ could be used to assess the variation in ϕ_i with respect to ϕ.

One approach is to use the discrete Fourier transform to separate the effects of each source. Once this is done, the difference in phase measured across the channels for a particular frequency component then gives the variation in phase of (13) for a single

multipath source. If the analysis is restricted to the higher spatial frequencies (i.e. the lower frequencies associated with multipath sources around the receiver are ignored), then this approach provides a means to assess the size of the multipath region in the vicinity of the transmitter.

In reality, the spatial frequencies do vary as the transmitter moves making the separation of multipath effects in the spatial frequency domain only approximate. Nonetheless, the amount of separation is sufficient for the purposes discussed here. For example, after transforming the simulation data shown in Figure 23a-d to the spatial frequency domain, the relative phase values (referenced to channel 0) are plotted in Figure 26 for the frequency bins in the range 0.4 to 1.26 cpw. As expected, the greater the diameter of the transmitter multipath regions, the larger the spread in phases.

A simple way to quantify this effect is to average the absolute value of the phase in channel $K-1$ (measured relative to channel 0) over the given range spatial frequencies. Mathematically,

$$\overline{|\theta_{K-1}|} = \frac{1}{N2 - N1 + 1} \sum_{n=N1}^{N2} \theta_{K-1}(f_n) \tag{14}$$

where $\overline{|\theta_{K-1}|}$ is the averaged phase value, $\theta_{K-1}(f_n)$ is the phase for spatial frequency f_n measured in channel $K-1$ relative to channel 0, and $N1$ and $N2$ are the bin numbers corresponding to the minimum and maximum spatial frequencies over which the results are to be averaged. Ambiguities in the value of $\theta_{K-1}(f_n)$ of the form $m2\pi$ for $m = 0, \pm1, \pm2, ...$ are resolved by unwrapping the phase using the phase differences $\theta_k(f_n)$ for $k = 1, 2, ..., K-2$.

Using the phase averaging approach to quantify the multipath induced phase spreading, the results for 200 different simulations (50 for each model) are shown in Figure 27. The results indicate that the multipath models can be distinguished through appropriate processing of the measurement data. The difference between the results of model 2 and model 3 are very small, particularly given the differences in the respective multipath regions illustrated in Figure 24b and c which would lead one to expect the phase spreading for model 3 to be smaller than they are.

The explanation for the higher than expected spreading is that in the simulations using model 3, a larger portion of the significant multipath power was generated along the direct signal path than compared to simulations using model 2 (see Figure 24). Since the phase spreading calculation removes these direct path multipath sources, the multipath sources in the vicinity of transmitter, but outside the region of "significance", have a greater

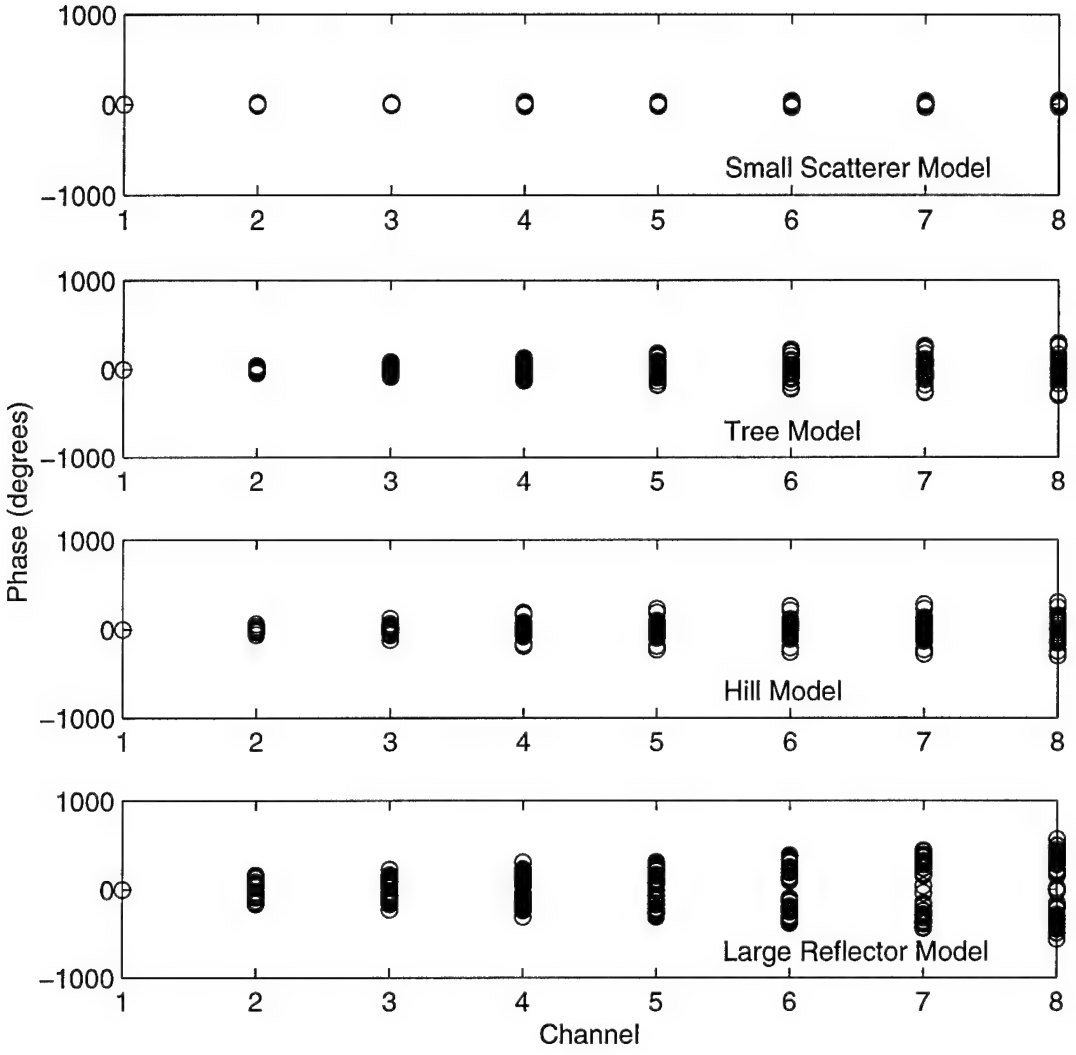

Figure 26: Phases measured across all channels for spatial frequencies from 1.4 to 1.26 cpw. One example from each simulation set is shown.

influence than would be expected otherwise resulting in greater phase spreading. An examination of the relative levels of the lower spatial frequencies (i.e. < 0.1 cpw) could be used to differentiate the model 2 results from model 3, but this was not found to be necessary.

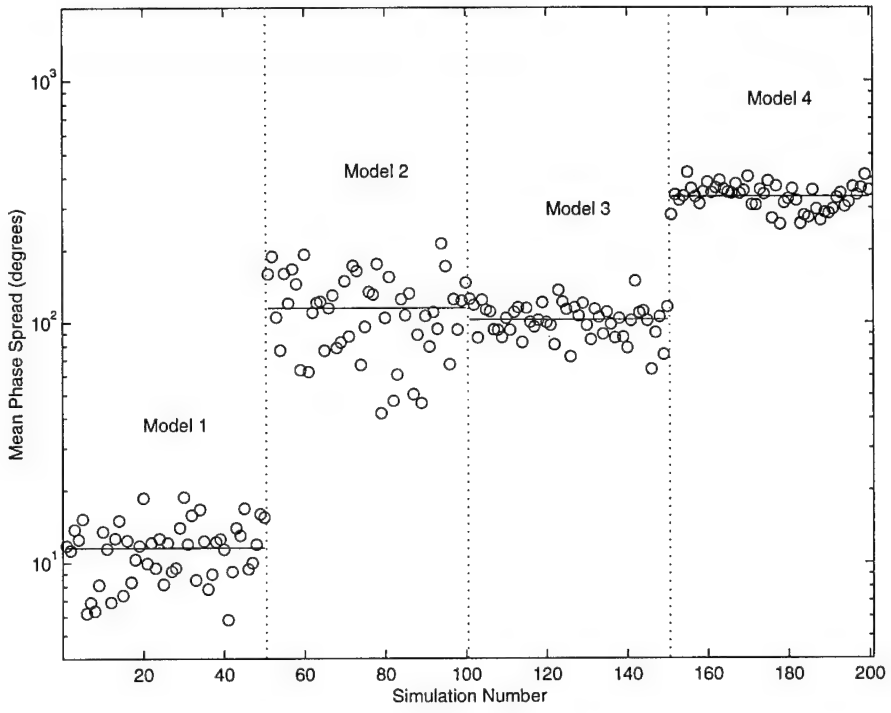

Figure 27: Average phase spread for 200 simulation examples.

5.4 Refining the Multipath Model

Having developed a method which can assess the relative diameter of the multipath region in the vicinity of the transmitter, the next logical step is to use this method to process the measured data. Using measurement sets 1 to 4 and 7 to 14 for this assessment, the results are shown in Figure 28 with an average value of 43°. The results were omitted for measurement set 5 since the transmitter was stationary, for measurement set 6 since the accuracy of locating the transmitter was poor, and for measurement sets 15 to 18 since the transmitter-receiver distances were considerably different than used in the simulations (the effect of longer/shorter paths is dealt with in Section 6.1).

Comparing the results in Figure 28 to those results shown in Figure 27, the results for the real environment lie somewhere between the model 1 and model 2 results.

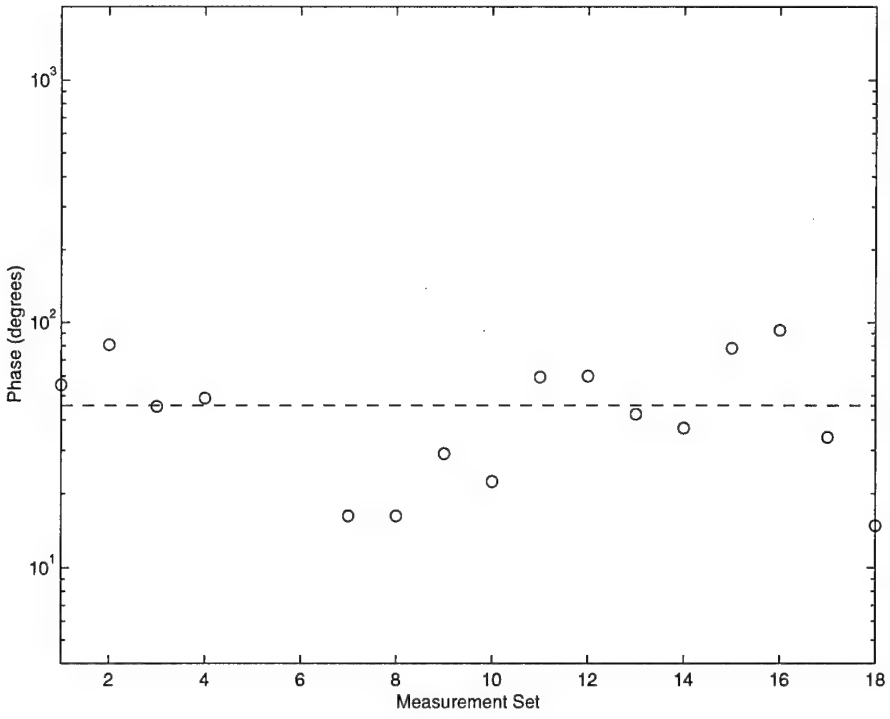

Figure 28: Average phase spread for the field trial measurements.

To refine the estimates, scaled versions of model 2 were used to simulate objects with sizes ranging from that of model 1 to the original model 2. Some examples of the scaled model are shown in Figure 29. By generating sets of 50 multipath simulations for each variation of model 2, it was found that the version shown in Figure 29c produced similar average phase spreading results (49°) as the real data. This particular version is denoted model 2x. An example of the simulated power and bearing error outputs, compared with the same measurements for measurement set 12, are shown in Figure 30.

Previously, the most significant sources of multipath were identified as the strongest sources which together produced 99.9% of the total multipath power. This is equivalent to ignoring all the weakest multipath sources which together produce 0.1% or less of the total multipath power. For DF purposes, a very similar but slightly more useful measure is to ignore the weaker multipath sources whose combined effect results in less than a given RMS bearing error, say 0.1°. The main difference between the two measures of significance is that the first measure is relative while the second measure is based on a hard limit. The relative measurement is useful for determining the shape of the multipath regions independent of the density of the sources of multipath (lower density environments can be simulated more easily). The bearing limit approach ensures that only multipath

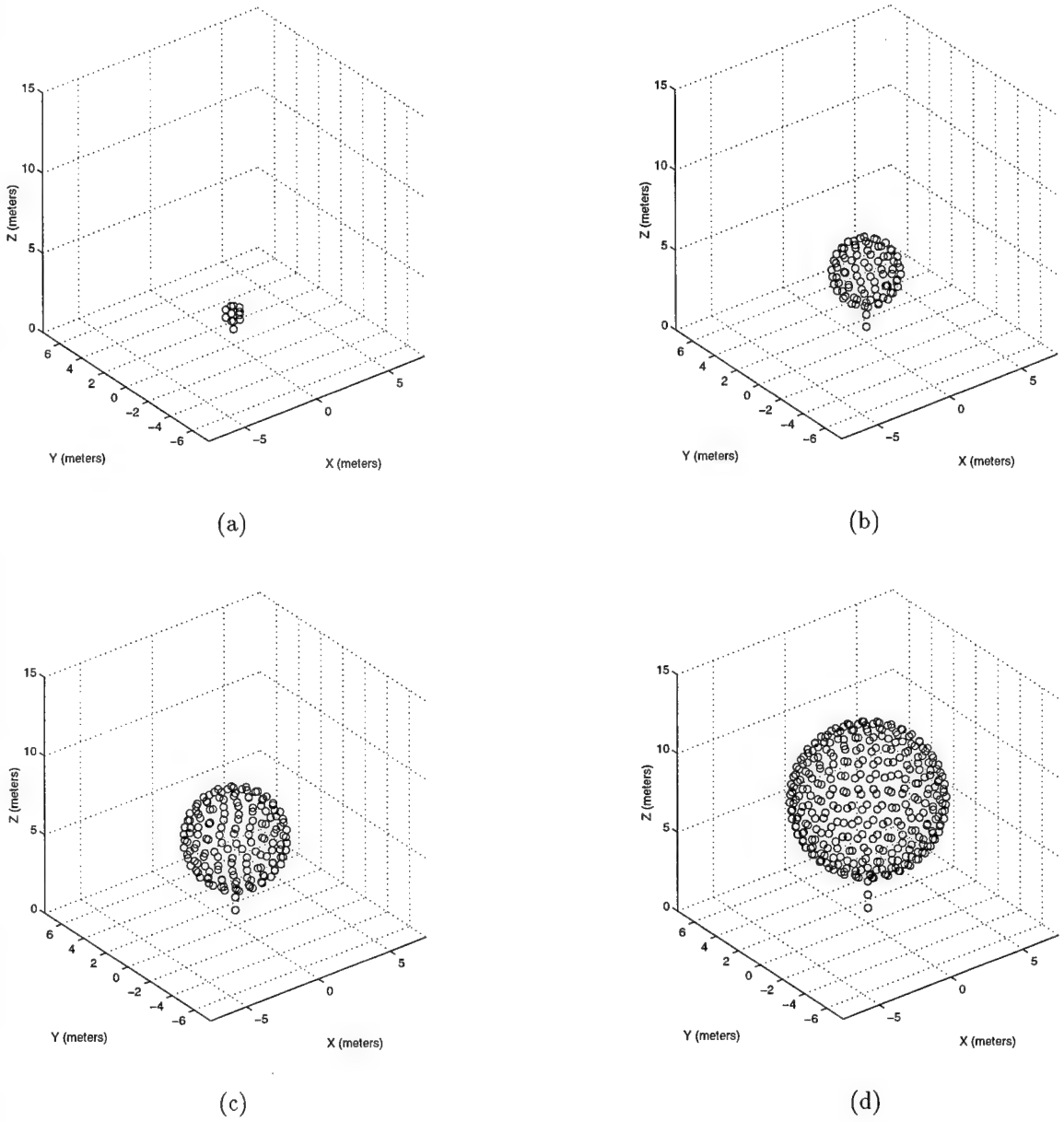

Figure 29: Scaled versions of the tree model with diameters of (a) 0.75m, (b) 3.8m, (c) 5.7m, and (d) 8.6m (model 2).

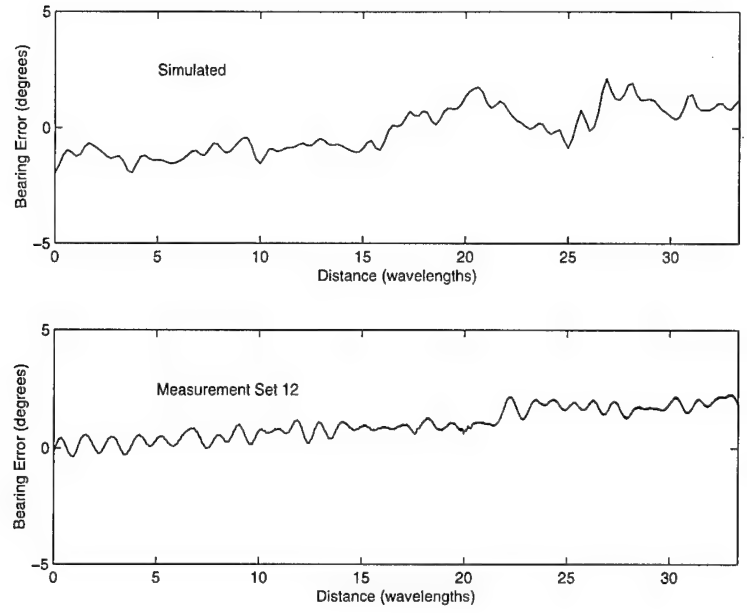

(a)

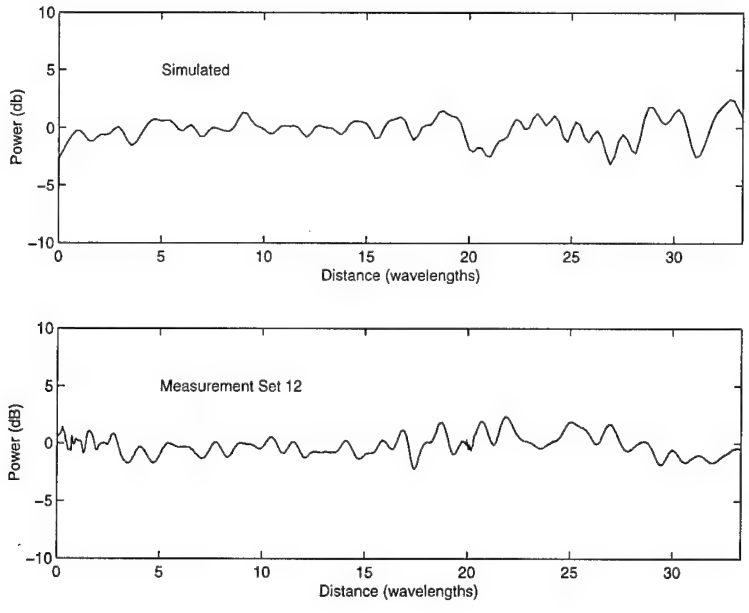

(b)

Figure 30: Comparison of a simulation using model 2x with measurement set 12 showing (a) bearing error, and (b) received power.

sources capable of causing objectionable errors are considered; in this case, the size of the multipath region will be affected by the density of the multipath sources.

For the 50 simulations involving model 2x, the density of multipath sources was set to produce signal-to-multipath power ratios of between 0 to 15 dB which were higher than the previous simulations. At these power levels, the power and bearing error results were similar in magnitude to the real world results making comparisons easier as shown in Figure 30. Using the bearing limit approach and super-imposing the locations of the significant multipath sources for all 50 simulations involving model 2x yielded the multipath regions shown in Figure 31.

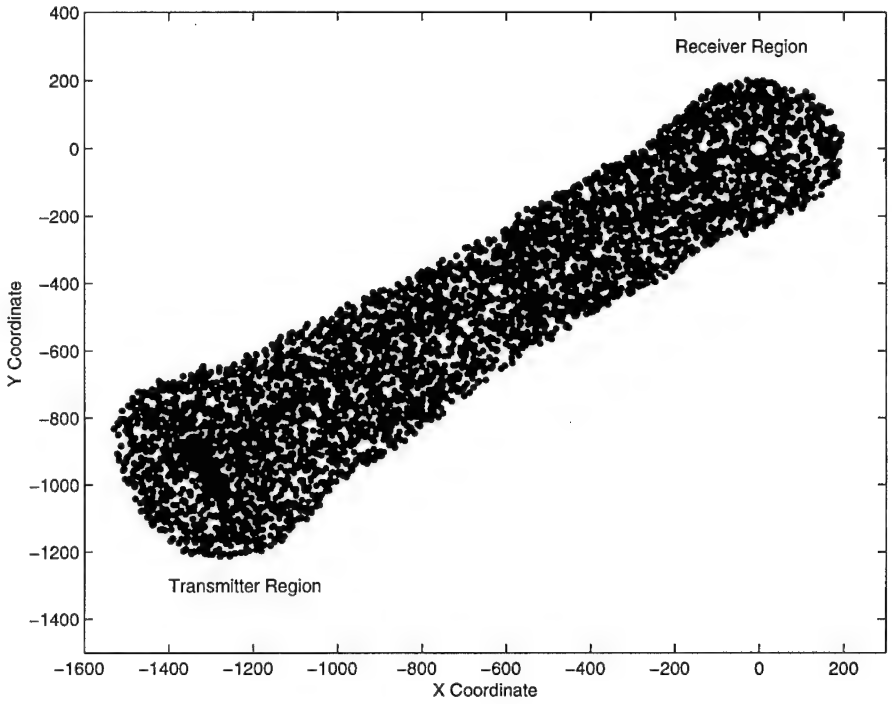

Figure 31: Positions of most significant multipath sources for the 50 simulations using model 2x.

With the multipath regions defined in Figure 31 as the reference, the average number of significant multipath sources was found to be 101. Although there are some obvious deficiencies in these simulations as will be discussed in the next section, it would not be unreasonable to conclude that DF systems in the real-world must contend with a large number of multipath sources on the order of 100.

6.0 EXPLORING FACTORS AFFECTING DF

Up to this point, it has been shown that a simple simulation model employing a large number of identical tree-like multipath sources was sufficient for reproducing most of the effects seen in the field trial data. In the rest of this section, this model is used to investigate various factors which affect DF including: increasing/decreasing the transmitter-receiver path length, clearing the DF site of obstacles causing multipath, raising the DF antenna array, and choosing/modifying the DF algorithms. The last three factors are of particular interest since they are under direct control of the DF site.

Before proceeding with this investigation, it is important to put the modelling results in perspective. For example, the density of model trees (model 2x) required to produce the same RMS bearing errors and power ripple observed for the field measurements works out to 1.3 trees per 100m x 100m square or one tree every 77 meters. Although a quick visual survey of the area around DREO indicates that trees are the most prominent feature, the actual density would appear to be somewhat higher than the modelled density. This is partly due to the fact that the model considers significant multipath sources only, whereas the DREO site contains trees and bushes of all shapes and sizes, some of which will cause significant multipath and some of which will not. A second reason is that the trees in the model tended to be more uniformly distributed whereas the trees on the DREO site tend to be more clustered. Clusters can be modelled by a fewer number of strategically placed trees. A third reason is that the model trees are electrically opaque (i.e. metallic trees) whereas real trees are better represented by a dielectric block (not opaque). The model tree will then have a greater effect than its similarly sized real-life counterpart. The main implication here, is that the value of 100 for the number of significant multipath sources is probably too low.

Another consideration is the effect of large scale terrain features such as hills or mountains. The area around DREO is relatively flat with the elevation changes over the measured signal paths typically less than 20 meters. As a result, there was little opportunity to observe the effects of large scales features except in a couple of instances as will be discussed later on.

More sophisticated simulations could have been developed (e.g. using various sized and shaped multipath sources in each simulation, and allowing clustering), however the extra effort was not deemed warranted. As a consequence, the results given in the following discussion should not be considered "exact", but taken as reasonable estimates.

6.1 Transmitter-Receiver Path Length

Up to this point, the simulations have involved transmitter-receiver path lengths of approximately 1.6 km. While this was appropriate for analyzing measurements made for the bulk of the measurements made on or near the DREO site, it is natural to ask whether the simulation results are also appropriate for longer path lengths.

To investigate this question, 50 simulations using model 2x were run using the geometry from measurement 17 but limiting the transmitter to the central 160 meters of the route shown in Figure 16a. In this case the transmitter-receiver path length was approximately 5.3 km. The terrain along the direct signal path was very similar to the terrain around DREO; namely, rolling with an elevation deviation of less than 20 meters, relatively open with scattered trees, groves of trees, and woods. Given the previous results, model 2x would seem to be a good match for this terrain. At first glance, this does not appear to be the case for the results shown in Figure 32 which compares the power and bearing from one simulation with the corresponding subset of measurement set 17. The main difference is a strong ripple component with a relatively constant spatial period seen in the field measurement data but not the simulations. Given that this ripple component corresponds to a relatively high spatial frequency of 0.9 cpw indicating multipath generated in the vicinity of the transmitter, and given similar observations for measurement sets 1 and 2, the conclusion is that the sources of multipath were the large trees lining the side of the road and blocking the direct signal path. This was not properly modelled in the simulations due to the spacing restriction imposed.

Further justification for the tree conclusion comes by comparing the large rapid power oscillations in measurement set 17 to the more subdued power variations found in measurement set 18 (see Figure 16). The main physical difference between these two sets was that for measurement set 18, there were no large trees close to, and directly in front of/behind, the transmitter since the transmitter was moving down the road directly away from the receiver (i.e. there were no trees growing on the road). Hence the transmitter had a clearer view of the receiver compared to the more obstructed view for measurement set 17.

It is also worth pointing out the differences in the slower power variations between measurement set 17 and 18. In measurement 18 there is an increase in received power of approximately 10 dB from the beginning to the end of the measurements which is consistent with the fact that the transmitter was moving uphill (pathloss decreases with

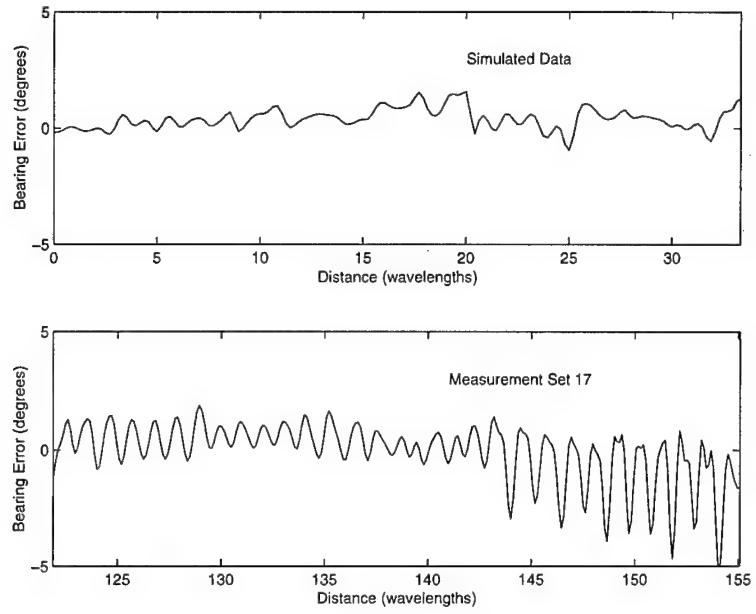

(a)

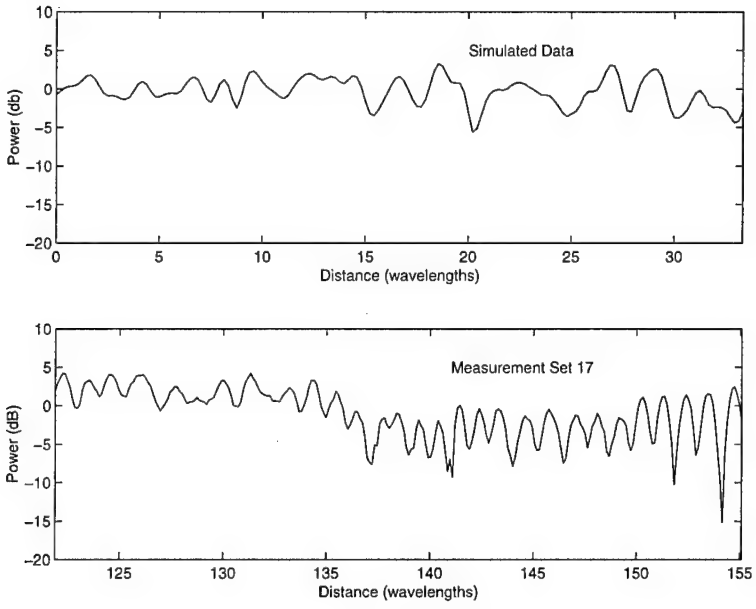

(b)

Figure 32: Comparison of the results from a simulation using model 2x with the corresponding results from measurement set 17 showing (a) bearing error, and (b) received power.

elevation at low elevations). In measurement 17, the large slow variations – a drop of almost 15 dB from 0λ to 150λ, an increase of nearly 15 dB from 150λ to 250λ, and a drop of 10 dB at 270λ – cannot be related to transmitter elevation but was more likely due to shadowing by very large obstructions closer to the transmitter than the receiver and on the order of 100λ long (e.g. woods). Alternatively, the large slow variations in measurement 17 may have been caused by multipath sources closer to the receiver, although the rapid drop at 270λ tends to favour the explanation of an obstruction nearer the transmitter.

A more effective way to compare the simulated and field trial data, instead of using Figure 32, is by comparing average phase spreading values since one strong spatial frequency component will not dominate the results. Performing the calculations for the simulated data yields an average phase spreading value of 17°. To compare with the real world values, measurement set 17 was divided into subsets representing consecutive 160 meters stretches of the transmitter route. Processing these subsets yielded an average result of 20.4° which is slightly higher than the simulation results.

Given the apparent agreement between the field measurement and simulation results, the next consideration is how the size and shape of the multipath regions change as the transmitter-receiver distance changes. Overlaying the locations of all significant multipath sources (using the 0.1° RMS bearing error criteria), the multipath regions for the simulations are shown in Figure 33. Comparing this to Figure 31, the main effect of increasing transmitter-receiver distance is the reduction of the contribution of multipath sources in the region encompassing the midpoint of the direct signal path. The regions around the transmitter and receiver are relatively unaffected in shape and size (e.g. the receiver region is approximately 400 meters across in both cases), and the average number of multipath sources for the 50 simulations (108) was also relatively unaffected.

One implication of the apparently constant number of significant multipath sources for the larger transmitter-receiver distances is that it provides an opportunity for larger, less densely spaced multipath sources to provide a greater relative contribution. For example, a sufficiently large multipath source could affect the signal all along the direct signal path. Hence for a given density, the longer the path the greater the number of these larger multipath sources and the greater their relative effect. This may explain the slightly higher phase spreading observed for measurement 17 compared to the simulation results (since greater phase spreading is expected for large sources of multipath).

The analysis for the 5.3 km range was also repeated for measurement set 16 where the mean transmitter-receiver distance was only 106 meters. In this case, the transmitter

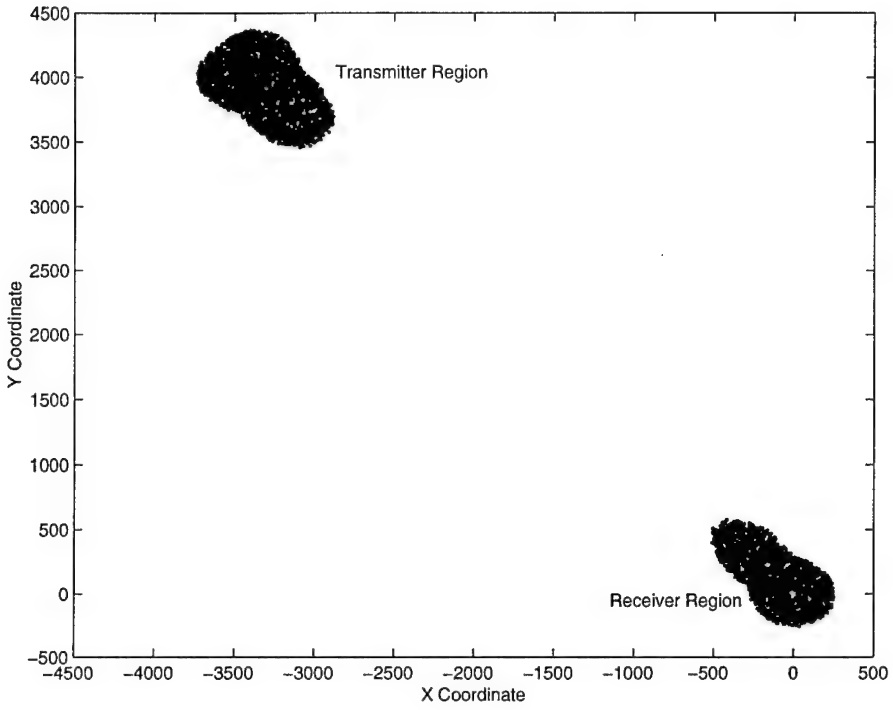

Figure 33: Positions of most significant multipath sources for the 50 simulations using model 2x and the 5.3 km transmitter-receiver path.

route used in the simulations was the same as for the real world measurement. After processing the data the average phase spread for the 50 simulations was a remarkable 401° as compared to 116° for measurement set 16 (the data was not subdivided in this case). Using smaller sized sources (such as model 1) reduced the phase spread in the simulations but the discrepancy between the simulated and actual results was still very large (over 70°).

To investigate whether the lower phase spread for the real measurements was due to the particular site layout, a simulation was set up where the simulated trees (using model 2x) were located in approximately the same places as the actual trees based on overhead photography but ignoring small trees and bushes. Figure 34 shows these locations. A comparison of the power and bearing error output for this simulation with measurement set 16 is shown in Figure 35. Although the real and simulation results differ (which is expected since only a single sized tree type was used in the simulation), qualitatively, in terms of their spatial frequency content and the magnitude of variations in power and bearing, they appear similar. The average phase spread for the simulation was found to be quite sensitive to the positions of the multipath sources closest to the DF receiver antenna array, with changes of only a few meters causing variations in phase spreading

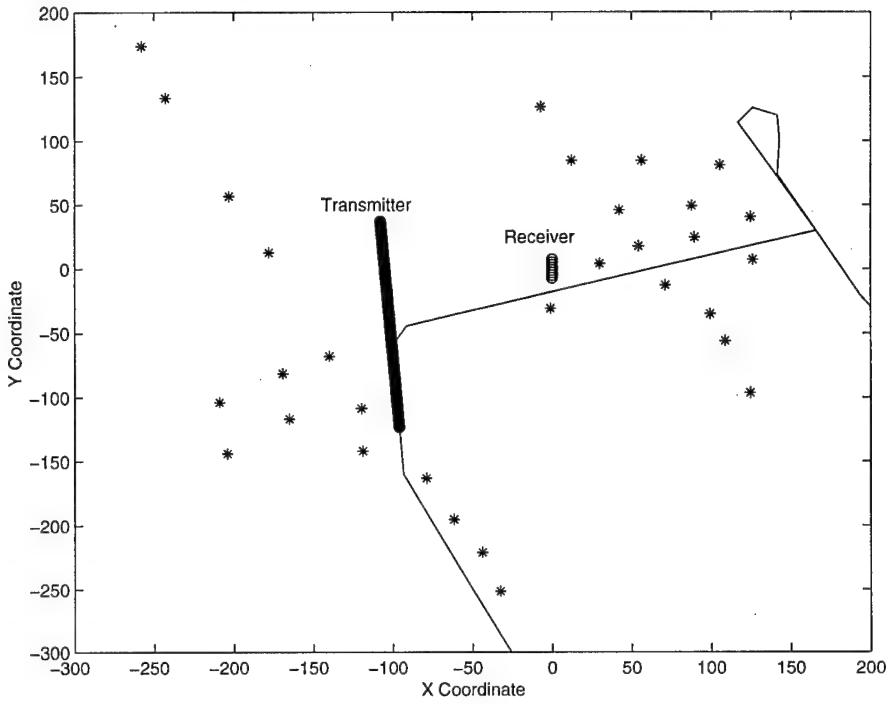

Figure 34: Positions chosen for simulated trees (model 2x) based on overhead photography of site.

values of from 70° to 200°. For the example shown here, the average phase spread value was 119° which is in close agreement with the actual value of 116°.

Having shown that model 2x produces reasonable results at close ranges, Figure 36 shows the locations of all significant multipath source locations used in the simulations. Due to the close range and the effect of path losses, the transmitter and receiver multipath regions have merged and shrunk to 200 meters across (measured through the receiver). The resultant average number of significant multipath sources was only 9 in this case.

The last range effect examined here is accuracy. Based on Figures 31, 33, and 36, accuracy would be expected to improve as range increases since the angle subtended by the multipath sources in the transmitter region decreases with range. A reasonable measure of this effect would the standard deviation of the bearing errors (i.e. the RMS error after the mean error has been removed) since any mean error will be caused by multipath sources at the receiver site (or due to other sources of measurement error) which are not of interest here. The results of the standard deviation calculations are shown in Table 2 for both the simulated results and the field trial results. Wild bearings were removed from the calculations (wild bearings are defined in this report as those bearings in error

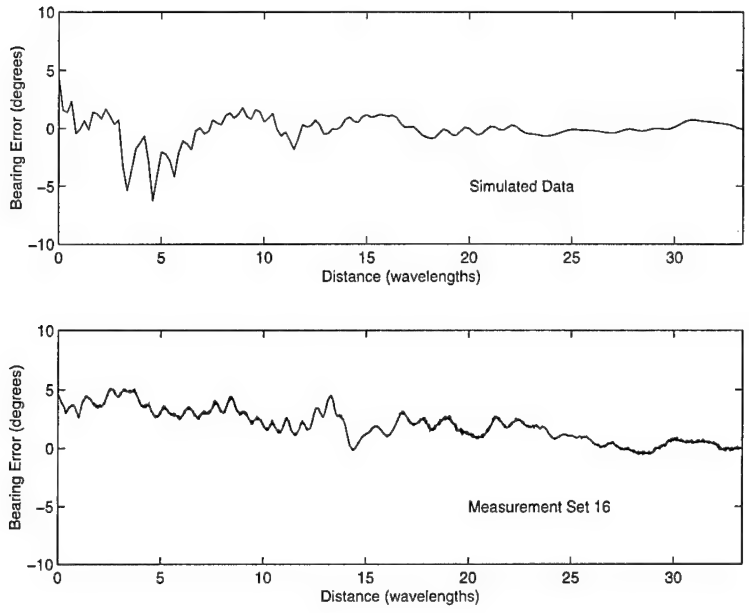

(a)

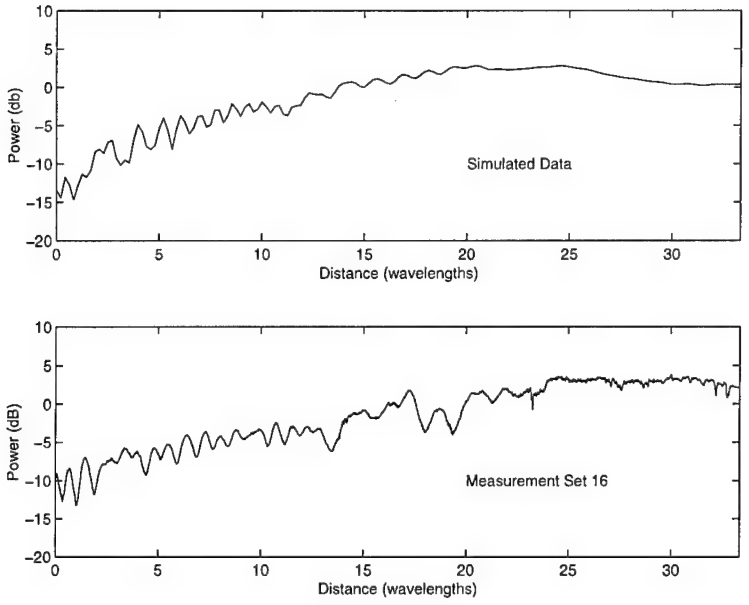

(b)

Figure 35: Comparison of the results from a simulation using model 2x with the corresponding results from measurement set 16 showing (a) bearing error, and (b) received power.

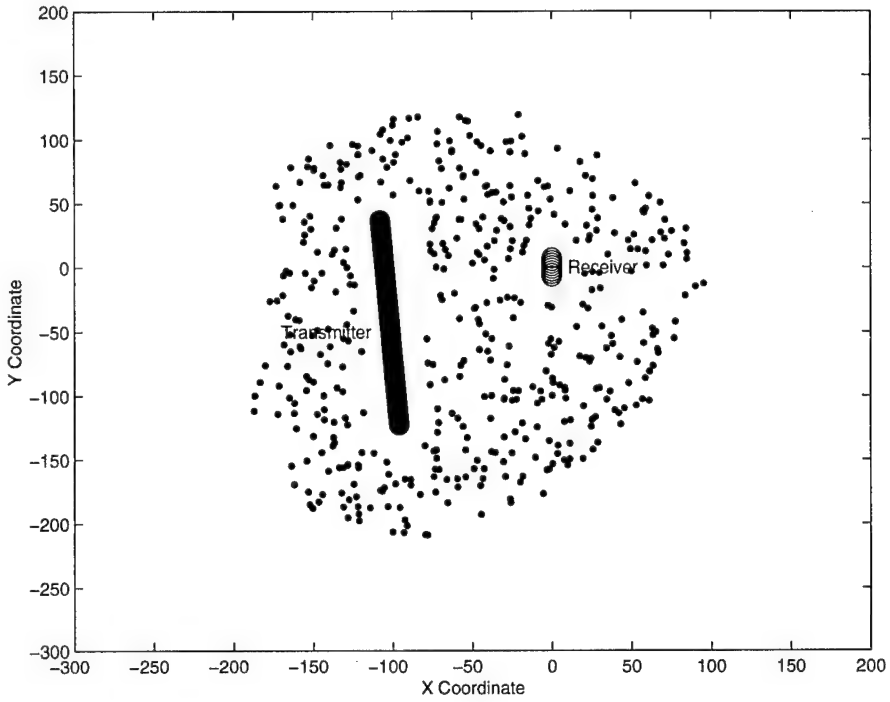

Figure 36: Positions of most significant multipath sources for the 50 simulations using model 2x and the mean 106 meter transmitter-receiver path.

by more than half the beamwidth of the Osprey DF array, i.e. $> 7.7/\cos\phi$ degrees, where ϕ is the transmitter bearing). For the simulated results, the standard deviations were computed from all 50 simulations generated for the appropriate range value. For the field trial results, the 106 meter range value was calculated using measurement set 16, the 1.6 km range value was calculated using measurement sets 1, 3, 9, 11, and 14, and the 5.3 km range value was calculated using measurement sets 17 and 18.

Table 2: Standard Deviation of Bearing Errors as a Function of Range

	Standard Deviation (degrees)	
Range	Simulated	Field Trials
106 m	2.1	1.3
1.6 km	1.2	0.7
5.3 km	0.7	0.7

The results in Table 2 indicate that there is some improvement with range, although perhaps not as much as predicted by the simulations. For the field measurements there was no apparent improvement from 1.6 km to 5.3 km. This may be a result of larger sized multipath sources having a greater effect as discussed previously. Unfortunately,

in this case, the field measurement data was too limited to make a more comprehensive assessment.

6.2 Clearing the DF Site

The analysis to this point, clearly indicates that a large number of sources contribute to multipath. In the past, DF algorithms which can simultaneously estimate the bearings of a number of signals (called superresolution algorithms) have been suggested and investigated as a possible solution to this problem [4]. Since these algorithms are limited to a theoretical maximum of $2N/3$ coherent signals or less, where N is the number of antennas in the DF array, a very large number of antenna elements would be required to deal with the multipath problem. For example, based on the simulations using model 2x, an array of well over 150 antennas would be required. This is clearly impractical and prohibitively expensive, especially for tactical systems.

An alternate approach would be to choose a clear receiver site, which would at least eliminate the effects of multipath sources near the receiver (but not the transmitter) and hopefully improve DF accuracy. To test this approach, the simulations used to generate the results for comparison with measurement set 17 were rerun with the area around the receiver array cleared out to varying distances. The overall RMS bearing error for each cleared distance was then calculated and the results for all cleared distances plotted in Figure 37.

Conventional wisdom suggests that the more the site is cleared the better the expected DF accuracy, which is exactly the case for the results plotted here. Taking a closer look at the results, the plot shows that clearing the receiver site out to a radius of 75 to 100 meters substantially improves the bearing accuracy, and that beyond 200 meters the improvement is minimal (i.e. 0.1° RMS or less). The plot also indicates the effect of wild bearings (the dashed line) when they are included in the RMS calculations.

One thing that this curve shows is the relative importance of the receiver and transmitter multipath regions. Completely clearing the receiver region reduces the bearing error from 3° to 0.5° RMS. In other words, the receiver region contribution to bearing error is considerably more than transmitter region. This is fortuitous since usually the choice of the receiver region can be controlled while the transmitter region cannot.

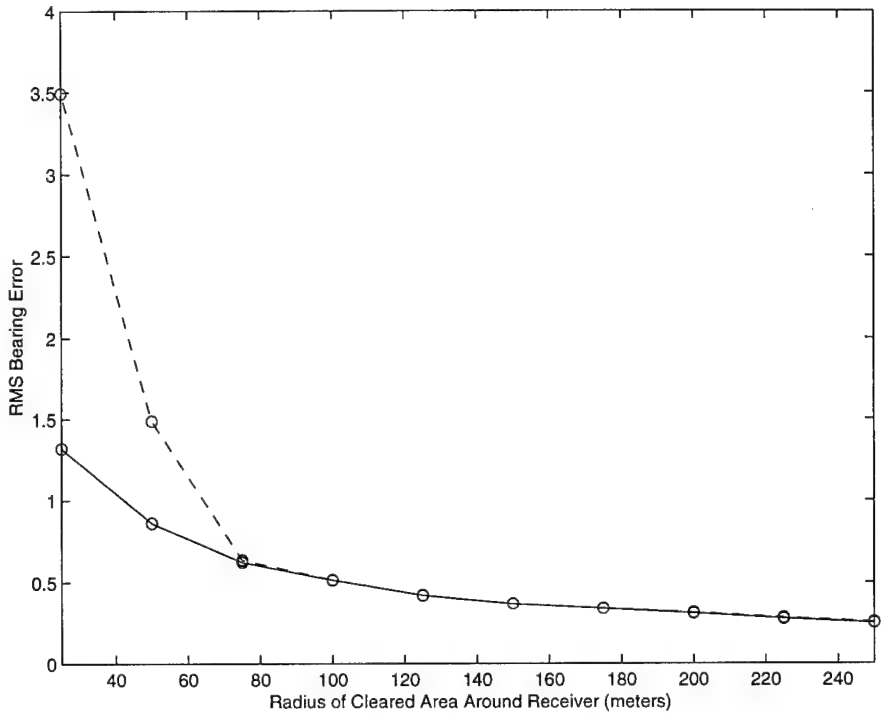

Figure 37: Effect of clearing the site around the receiver array on DF accuracy. The dashed line shows the result when wild bearings are included in the calculations.

The size of the multipath source also affects the results. For example, based on comparing the various region sizes in Figure 24, it might be expected that for small scattering sources, accuracy would improve faster as a function of clearing radius than for larger sized multipath sources. Performing the appropriate simulations for model 1 leads to the expected results (wild bearing excluded) which are shown in Figure 38 along with the simulation results for model 2x. In this case, a log-log scale was used which allows the differences to be more easily discerned. Additionally, the RMS bearing errors have been normalized to 1.0° at a distance of 25 meters to make the comparisons more relevant.

Examining the way errors begin to rapidly increase as the clearing radius decreases, it seems evident that under 25 meters DF errors may become prohibitively large. Given that this assessment is based on statistical results, for any particular site this trend may not necessarily be true (e.g. for the Osprey field measurements there were trees at closer distances), but it will be true in general. The possibility of large bearing errors for an uncleared site does underscore the need for careful DF site selection.

If both covert operation (e.g. that antenna array hidden in the trees) and high accuracy are high priorities, then calibrating the antenna array will be necessary. In theory,

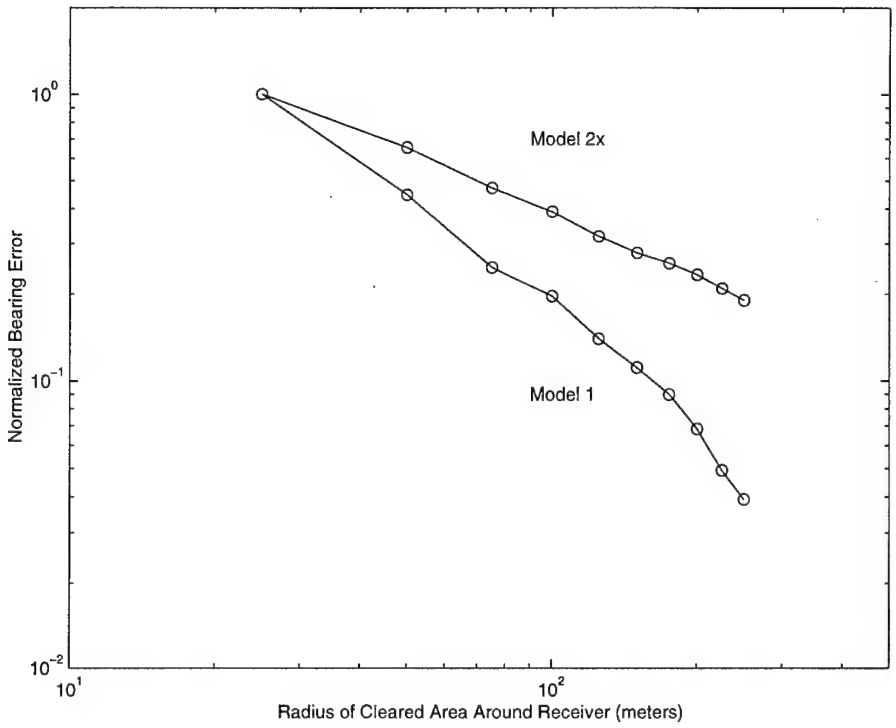

Figure 38: Comparison between models 1 and 2x of clearing the site around the receiver array and the effect on bearing error.

calibration could be used to compensate for multipath sources out to a given distance r. Based on the findings in this report and the conventional approach to antenna array calibration, the most obvious way to do the calibration would be to measure the antenna array response using a reference transmitter moved in a circle around the DF array (or at least in an arc covering the angular field of interest) with a radius several times r and with measurement points at spacings of $\lambda/2$. Spatial frequency processing would then be used to remove the effects of multipath sources at distances greater than r.

In practice, the utility of this calibration approach would be limited to compensating for multipath sources very close to the antenna array since the amount of effort required increases as the choice of r increases. For example, using $10r$ as a reasonable choice for the radius of the measurement circle, compensating for multipath sources within 25 meters at a frequency of 62.5 MHz would require $2\pi(10r)/(\lambda/2) = 655$ individual measurement points on the circle around the DF array. Hence for a tactical system, even $r = 25$ meters might be hard to justify in terms of time and effort.

6.3 Effect of DF Antenna Height

Another approach to achieving better DF accuracy is to raise the DF antenna array to provide a clearer field of view. Repeating the simulations for measurement 17 using different antenna heights, yielded the results shown in Figure 39. These results show that increasing antenna height improves DF accuracy. Additionally, examining the results in detail reveals that the behaviour of the solid curve above and below a height of 10 meters is different, with the greatest improvement in accuracy occurring just above 10 meters. This 10 meter value corresponds to the height of the trees suggesting that it is better for the DF antenna array to be higher than the surrounding trees.

Although these results do not take into account polarization effects, or different size and shapes of multipath sources, the general conclusion that higher is better – particularly in terms of exceeding the height of the surrounding trees – is in complete agreement with conventional wisdom. Additionally, extrapolating the results to a much greater height suggests that very high accuracy (0.1° RMS) is potentially achievable on an airborne platform.

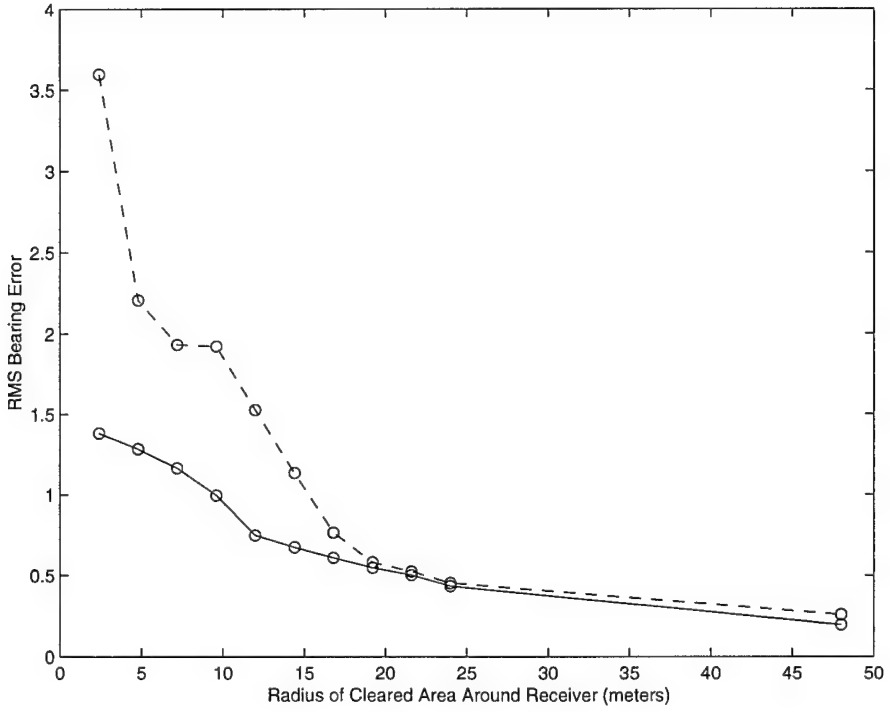

Figure 39: Effect of raising the DF antenna array on DF accuracy. The dashed line shows the result when wild bearings are included in the calculations.

6.4 DF Algorithm Performance

In the DF field trials reported in [4] and [5], the performance of a number of DF algorithms was tested. Against a single transmitter, most algorithms provided the same performance. For two or more transmitters operating simultaneously, however, the coherent eigen estimator (CEE) exhibited the best performance. The root-MUSIC algorithm also performed well, but surprisingly, the Maximum Likelihood approach (ML) did not. The implication is that the ML approach is not optimized for the spatial "noise" that multipath produces, while somehow, CEE and root-MUSIC are better suited.

In this section, the performance of these algorithms is again tested against two transmitters using both simulated data and real data. The purpose is to see if the results observed with the real world data can be reproduced by the simulations, and if so, what this implies about the performance of these DF algorithms when multipath propagation is present.

Since the measurement sets described in this report involved only a single transmitter, two transmitter measurements were created artificially using:

$$\mathbf{Y} = \frac{\mathbf{x}_i \mathbf{a}_i^H}{|\mathbf{x}_i|} + \frac{\mathbf{x}_j \mathbf{a}_j^H}{|\mathbf{x}_j|} \tag{15}$$

where $\mathbf{Y}$ is the two signal data matrix, $\mathbf{x}_k$ is the sensor snapshot for transmitter position k, and $\mathbf{a}_k$ is the complex transmitter modulation vector. The vectors $\mathbf{a}_i$ and $\mathbf{a}_j$ were chosen to be 1024×1 uncorrelated Gaussian noise sequences. The values of i and j were chosen according to the desired angular separation between transmitters, and $\mathbf{x}_i, \mathbf{x}_j$ could be chosen from the same or different data sets.

Drawing from measurement sets 1, 7, 9, 11-14, to generate two signals measurements, the three DF algorithms, CEE, root-MUSIC and ML, were tested and the results shown in Figure 40. The results were calculated for every 0.5° of separation between the transmitters from 2° to 20°. For each separation angle, 100 two signal data matrices were generated and then processed. The upper plot in Figure 40 shows the RMS error for each estimator as a function of the separation angle. The lower plot shows the corresponding failure rate, i.e. the percentage of time that one or both estimates of the two signals bearings were wild. As was observed in previous field trials, CEE exhibited the best performance (lowest RMS error and lowest failure rate for the smaller angular separations). However, in this case, root-MUSIC performed worse than ML.

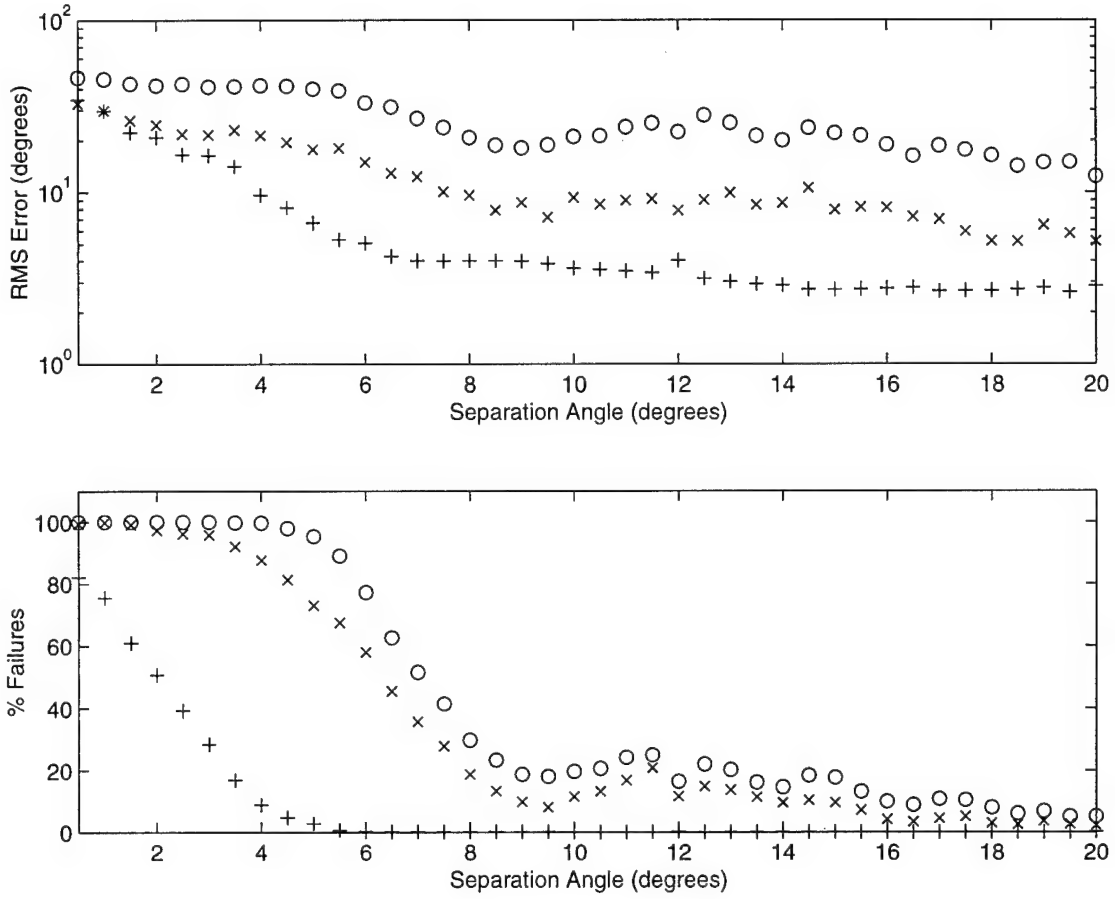

Figure 40: Comparison of three DF bearing estimators: ML ("x"), CEE ("+"), and root-MUSIC ("o") using field trial data.

Setting up a computer simulation with model 2x to reproduce the same angles and approximately the same transmitter-receiver path lengths as the appropriate field trials, the simulated data was processed to generate two signal data in the same manner as the real data. The results are shown in Figure 41. In this case, CEE and ML exhibited the same performance while MUSIC was the worst.

After some investigation as to why these results differed from the real data, it was found that the ML algorithm was more adversely affected by multipath sources close to the receiver array than CEE. Repeating the same simulation, but adding a smaller tree-like multipath source (6.7 meters high) near the endfire position of the DF antenna array (6 meters from the closest antenna and in a similar position to where smaller trees were actually located relative to the Osprey array), resulted in Figure 42 which shows CEE to have the best performance under these conditions.

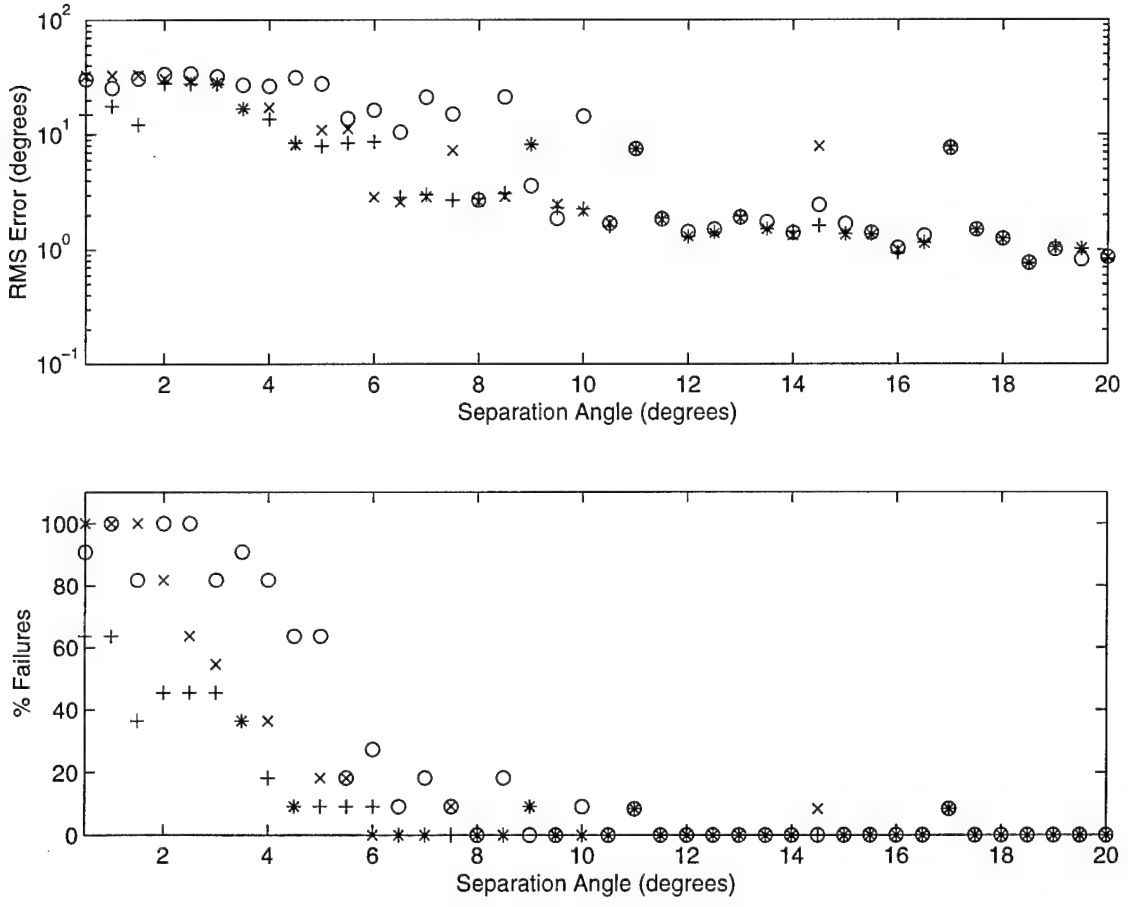

Figure 41: Comparison of three DF bearing estimators: ML ("x"), CEE ("+"), and root-MUSIC ("o") using simulation data.

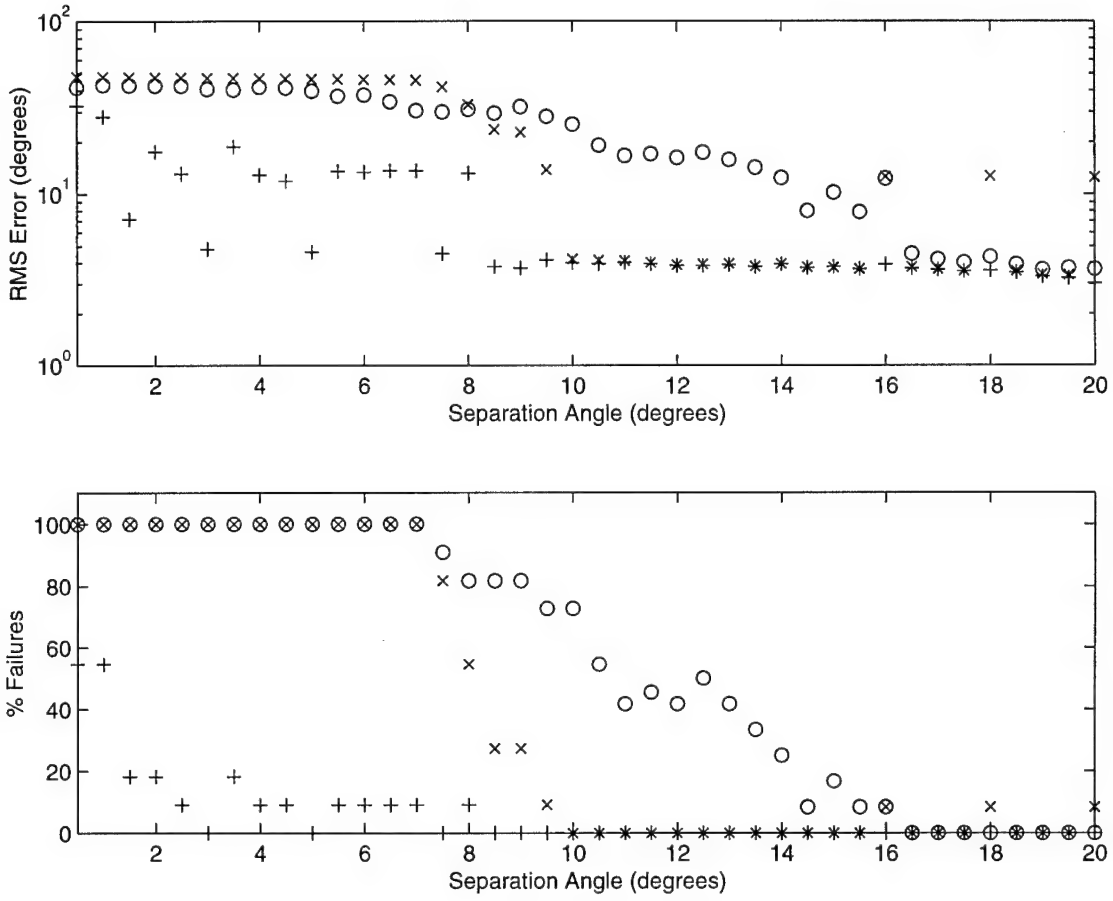

Figure 42: Comparison of three DF bearing estimators: ML ("x"), CEE ("+"), and root-MUSIC ("o") using simulation data generated with one of the multipath sources located near the endfire position of the DF antenna array.

From these results, it is quite obvious that not all DF algorithms perform equally. In this study and in previous studies ([4] and [5]), the CEE algorithm was the best performer owing to its greater immunity to multipath sources close to the receiver array. Against sources of multipath further out, the CEE algorithm did not appear to perform any better than the ML algorithm.

A natural question is whether DF algorithms be improved further. The answer is yes and this can be most easily explained using the ML algorithm as an example. Although optimal for signals with additive and uncorrelated white Gaussian noise, but no multipath, the ML algorithm is clearly not optimal for the signal environments explored here. The problem is that although the multipath signals can be treated as spatial noise, the statistical characteristics are not white Gaussian. For example, a simple inspection of Figure 31 is enough to reveal that most of the multipath power arrives from the approximate direction of the transmitter resulting in a coloured, not white, spatial noise spectrum. This directional nature also means that the multipath noise will be correlated from sensor to sensor, as well as correlated with the direct signal. Hence the ML algorithm would need to be reformulated to incorporate these multipath noise characteristics in order to achieve better accuracy.

Using a modified noise model, the greatest improvements would likely occur for co-channel signals situations where algorithm modelling errors have the greatest impact on accuracy. If modulation information is also incorporated into the estimator, such as for the modulation dependent algorithms studied in [4] and [5], the combined improvements could be quite significant.

7.0 CONCLUSIONS AND RECOMMENDATIONS

Based on a series of DF field measurements taken with the Osprey System in the relatively flat rural countryside surrounding DREO, RMS bearing errors were found to be typically on the order of one degree or more. These errors were predominantly due to the effects of multipath which were observed to be prevalent everywhere.

Simulation results determined that the dominant sources of multipath for the field measurements were the trees populating the country side. The trees having the most significant effect were those located in the regions surrounding the transmitter, receiver, and parts or all of the direct signal path. In the simulations, the required number of significant trees was typically on the order of 100 in order to generate similar levels of RMS bearing errors as observed in the field measurements. Due to limitations in the simulation approach, the number of actual trees affecting the field measurements was probably several times greater.

The simulation models were also used to investigate various factors affecting DF accuracy in a multipath environment. These factors included: the transmitter-receiver distance, the size of the clearing at the DF site, the height of the DF antenna array, and the DF algorithm.

From these investigations, accuracy was determined to improve as the transmitter-receiver distance increased. Comparing these results to the field measurements, this relationship was found to be true for distances less than approximately 2 km, but did not seem to hold up for greater distances. In fact, the accuracy at 5.3 km was observed to be the same as at 1.5 km. The most probable explanation for this discrepancy between the simulation and field trial results is that when the transmitter-receiver distance becomes sufficiently large, objects larger than trees (e.g. groves of trees, woods, etc.) begin to adversely affect the DF measurements. These larger multipath sources were not accounted for in the simulations.

Clearing the DF site of all multipath sources was found to improve DF accuracy, which is consistent with conventional wisdom. For a tactical system this procedure might be problematic due to time constraints and the requirement for covert operation. Calibrating the DF antenna array on site might provide a partial solution (calibration cannot compensate for multipath sources near the transmitter), but this approach is also time consuming. Even compensating for multipath sources located within 25 meters of the

antenna array would require an extensive number of measurements using traditional approaches. However, placing a DF array too close to trees or other sources of multipath without any sort of compensation could result in extremely poor accuracy or meaningless bearings.

Raising the antenna as high as possible above the surrounding sources of multipath was also found to improve accuracy, again consistent with conventional wisdom. Extrapolating from the simulation results indicates that airborne DF platforms could potentially achieve very high accuracy DF (0.1° RMS).

Finally, it was found that the choice of DF algorithm has an affect on accuracy. The CEE algorithm, based on the results here and in previous studies, was found to be the best of the modulation independent algorithms due to its greater immunity to the effects of multipath sources very close to the array. Even better DF algorithms could be developed by treating multipath as a noise phenomena and incorporating the appropriate statistics into the noise model of the algorithm.

Based on the findings in this report, there are several areas of research and development which could be pursued to achieve improved accuracy for tactical VHF DF systems. One area is improvement of calibration approaches to allow rapid characterization of the multipath sources around the DF antenna. A second area is the investigation of airborne DF platforms, since their height advantage could yield accuracies approaching 0.1° RMS. A third area is the improvement of DF algorithms which includes:

1. developing terrain modelling to correct for DF errors caused by large, easily identified terrain features such as forests, hills, mountains, etc.;

2. modifying the noise model used by the DF estimator to properly reflect multipath clutter generated by smaller objects (e.g. groves of trees, isolated trees, bushes, etc.) near the DF array, transmitter, and along the direct signal path; and

3. incorporating modulation dependent techniques to improve co-channel performance.

REFERENCES

[1] Read, W.J.L., "The Effects of the Environment on an Experimental VHF Radio Direction Finding Antenna System", Defence Research Establishment Ottawa, Report No. 1226, August 1994.

[2] Read, W.J.L., "Multipath Modelling for Terrestrial VHF Radio Direction Finding", Defence Research Establishment Ottawa, Report No. 1300, December 1996.

[3] "Navaids and Avionics Enroute Systems, Doppler VHF/DF, Site Selection", Publication No. C4-2VHF/DF-3, Telecommunications and Electronics Branch, Transport Canada, March 1, 1976.

[4] "Report on VHF DF Super-Resolution Field Trials held at Defence Research Establishment Ottawa", TTCP Report, September, 1994, CONFIDENTIAL.

[5] "Report on VHF DF Super-Resolution Field Trials held at Vint Hill Farms Station, Warrenton", TTCP Report, September, 1995, CONFIDENTIAL.

UNCLASSIFIED

SECURITY CLASSIFICATION OF FORM
(highest classification of Title, Abstract, Keywords)

DOCUMENT CONTROL DATA

(Security classification of title, body of abstract and indexing annotation must be entered when the overall document is classified)

1. ORIGINATOR (the name and address of the organization preparing the document. Organizations for whom the document was prepared, e.g. Establishment sponsoring a contractor's report, or tasking agency, are entered in section 8.)

DEFENCE RESEARCH ESTABLISHMENT OTTAWA
NATIONAL DEFENCE
SHIRLEYS BAY, OTTAWA, ONTARIO K1A 0Z4 CANADA

2. SECURITY CLASSIFICATION (overall security classification of the document including special warning terms if applicable)

UNCLASSIFIED

3. TITLE (the complete document title as indicated on the title page. Its classification should be indicated by the appropriate abbreviation (S,C or U) in parentheses after the title.)

MEASUREMENT OF MULTIPATH AND ITS EFFECTS ON TERRESTRIAL VHF RADIO DIRECTION FINDING (U)

4. AUTHORS (Last name, first name, middle initial)

READ, WILLIAM J.L.

5. DATE OF PUBLICATION (month and year of publication of document)	6a. NO. OF PAGES (total containing information. Include Annexes, Appendices, etc.)	6b. NO. OF REFS (total cited in document)
DECEMBER 1997	75	5

7. DESCRIPTIVE NOTES (the category of the document, e.g. technical report, technical note or memorandum. If appropriate, enter the type of report, e.g. interim, progress, summary, annual or final. Give the inclusive dates when a specific reporting period is covered.)

DREO REPORT

8. SPONSORING ACTIVITY (the name of the department project office or laboratory sponsoring the research and development. Include the address.)

DEFENCE RESEARCH ESTABLISHMENT OTTAWA
NATIONAL DEFENCE
SHIRLEYS BAY, OTTAWA, ONTARIO K1A 0Z4 CANADA

9a. PROJECT OR GRANT NO. (if appropriate, the applicable research and development project or grant number under which the document was written. Please specify whether project or grant)	9b. CONTRACT NO. (if appropriate, the applicable number under which the document was written)
5BD12	

10a. ORIGINATOR'S DOCUMENT NUMBER (the official document number by which the document is identified by the originating activity. This number must be unique to this document.)	10b. OTHER DOCUMENT NOS. (Any other numbers which may be assigned this document either by the originator or by the sponsor)
DREO REPORT 1325	

11. DOCUMENT AVAILABILITY (any limitations on further dissemination of the document, other than those imposed by security classification)

(XX) Unlimited distribution
( ) Distribution limited to defence departments and defence contractors; further distribution only as approved
( ) Distribution limited to defence departments and Canadian defence contractors; further distribution only as approved
( ) Distribution limited to government departments and agencies; further distribution only as approved
( ) Distribution limited to defence departments; further distribution only as approved
( ) Other (please specify):

12. DOCUMENT ANNOUNCEMENT (any limitation to the bibliographic announcement of this document. This will normally correspond to the Document Availabilty (11). However, where further distribution (beyond the audience specified in 11) is possible, a wider announcement audience may be selected.)

UNLIMITED

UNCLASSIFIED

SECURITY CLASSIFICATION OF FORM

DCD03 2/06/87

UNCLASSIFIED

SECURITY CLASSIFICATION OF FORM

13. ABSTRACT (a brief and factual summary of the document. It may also appear elsewhere in the body of the document itself. It is highly desirable that the abstract of classified documents be unclassified. Each paragraph of the abstract shall begin with an indication of the security classification of the information in the paragraph (unless the document itself is unclassified) represented as (S), (C), or (U). It is not necessary to include here abstracts in both offical languages unless the text is bilingual).

(U) This report details the investigation of VHF radio direction finding (DF) and the effects of multipath propagation for terrestrial paths. For this investigation, an eight-channel DF system was used to make field measurements of a transmitter as it was slowly moved along a designated route. This allowed the fine scale effects of multipath on the measured signal bearing and power to be observed - effects which had been previously observed as being noise-like in nature. Computer modeling was also used in order to develop simulations able to reproduce the effects observed in the field measurements. This has lead to the identification of the main sources of multipath, and a statistical assessment of their numbers and distribution. The computer models also allowed other factors affecting DF accuracy to be investigated which include: the transmitter-receiver path length, the size of the clearing at the DF site, the DF antenna height, and the DF algorithm. The main conclusions are that multipath is a major impediment to very high accuracy DF for terrestrial VHF DF systems, but that steps can be taken to mitigate its effects.

14. KEYWORDS, DESCRIPTORS or IDENTIFIERS (technically meaningful terms or short phrases that characterize a document and could be helpful in cataloguing the document. They should be selected so that no security classification is required. Identifiers, such as equipment model designation, trade name, military project code name, geographic location may also be included. If possible keywords should be selected from a published thesaurus. e.g. Thesaurus of Engineering and Scientific Terms (TEST) and that thesaurus-identified. If it is not possible to select indexing terms which are Unclassified, the classification of each should be indicated as with the title.)

MULTIPATH
VHF
DIRECTION FINDING
PROPAGATION
N-CHANNEL
BEAMFORMING
SIMULATION
COMPUTER MODELS
ANTENNA ARRAYS
MUSIC
MAXIMUM LIKELIHOOD